NASA TN D-162

7N-39
197223
87P

TECHNICAL NOTE

D-162

HANDBOOK OF STRUCTURAL STABILITY

PART VII - STRENGTH OF THIN-WING CONSTRUCTION

By George Gerard and Herbert Becker

New York University

NATIONAL AERONAUTICS AND SPACE ADMINISTRATION

WASHINGTON September 1959

1X

TABLE OF CONTENTS

W-122

NATIONAL AERONAUTICS AND SPACE ADMINISTRATION

TECHNICAL NOTE D-162

HANDBOOK OF STRUCTURAL STABILITY

PART VII - STRENGTH OF THIN-WING CONSTRUCTION

By George Gerard and Herbert Becker

SUMMARY

The stability of various forms of stiffened and sandwich plates which have been considered for the compression covers of thin wings is presented in terms of orthotropic plate theory. Design charts are presented and methods of evaluating the elastic constants associated with each type of plate are reviewed.

Buckling and failure of multiweb, multipost, and multipost-stiffened forms of beam construction are considered in terms of available theoretical and experimental results. The pertinent findings of minimum-weight analyses are presented throughout the report as an aid in design.

INTRODUCTION

A transition from stiffened-panel construction such as considered in Part V of this "Handbook of Structural Stability" (ref. 1) to plate construction represented by multicellular beams has been witnessed in the evolution of supersonic-airframe wing structures. This change has been necessitated by the thin wings and subsequent high loadings required for efficient performance in the supersonic speed regime.

The reviews contained in previous parts of the "Handbook of Structural Stability" have been concerned to a large extent with a considerable mass of test data and theory accumulated over a period extending through 25 years. The subject of the present part, thin-wing multispar construction, on the other hand, is much more recent, going back at most for approximately 10 years. Consequently, the material presented herein is often incompletely developed because of a lack of experimental data and general design information.

Various types of stiffening arrangements are of interest for the compression covers of multicell beams. Thick tapered plates are commonly

used, and plates stiffened longitudinally, transversely, and with grids as well as honeycomb- and corrugated-core sandwich plates are under active consideration. These configurations represent different types of orthotropic plates and the stability theory of such plates can be considered in rather general terms. Consequently, the section of this report following the symbol list is devoted to a review of orthotropic-plate theory.

General results of this theory applicable to compressive and shear buckling of orthotropic plates are presented in the section "Stability of Orthotropic Flat Plates." Since the various types of plates are characterized by different elastic constants, a discussion of methods of evaluating these constants is also presented.

Because of the relative simplicity of multiweb forms of beam construction, it has been possible to consider buckling and failure of such beams in rather complete detail instead of considering individual elements. Thus, in the section "Buckling and Failure of Multiweb Beams in Bending," strength analyses are presented for integral-, built-up-, and formed-channel multiweb beams.

Recent development of multicell beams has led to multipost and multipost-stiffener construction. The stability theory for these forms of construction is reviewed in the section "Stability of Multipost Beams in Bending" and available results on buckling and failure tests are summarized. From a design standpoint, the minimum rigidities required of the post and stiffener systems for them to act as effectively rigid members are often of interest. Such information is also presented in the section "Stability of Multipost Beams in Bending."

Again from the design standpoint, the results of minimum-weight analyses of the various forms of construction are of considerable importance. Where available, such data are presented in the section pertinent to the particular form of construction considered. In the section "Comparative Efficiencies of Thin-Wing Construction" these results are reviewed to establish the comparative structural efficiencies of the competing plate, web, and multicell forms of construction.

This investigation was conducted at New York University under the sponsorship and with the financial assistance of the National Advisory Committee for Aeronautics.

SYMBOLS

A area, sq in.

a length of plate, in.

b width of plate, in.

C coefficient

$\bar{C}$ shear rigidity, lb/in.

c_{ij} flexibility coefficients

$\bar{c} = D_{xy}/\left(D_x D_y\right)^{1/2}$

D plate cross-section rigidity, $Et^3/12\left(1 - \nu_e^2\right)$, lb-in.

D_s bending rigidity of sandwich plate, lb-in.

$D' = \nu_x D_y = \nu_y D_x$

d diameter, in.

E elastic (Young's) modulus, psi

E_s secant modulus, psi

E_t tangent modulus, psi

$E' = \nu_x E_y = \nu_y E_x$

$\bar{E}$ effective modulus, psi

e end-fixity coefficient

$F = \left(f/t_w\right)\left(b_w/t_w\right)^{1/8}$

f effective rivet offset distance, in.

G shear modulus, psi

G_c shear modulus of core, psi

G_s shear secant modulus, psi

h overall height of box beam, in.

h_c height between centroids of sandwich facings, in.

h_p	height of posts, in.
I	moment of inertia of stiffener, in.^{4}
K	deflectional-spring constant, lb/in.
k	buckling coefficient in compression
k_f	wrinkling-failure coefficient of multiweb beam
k_s	buckling coefficient in shear
L_t	length of plate between transverse supports, in.
M	bending moment, in-lb
m	exponent, or half wave length in length direction
N	axial loading, lb/in.
n	number of supports, or half wave length in width direction
p	pressure, psi; also rivet pitch, in.
Q	transverse shear flow
q	shear flow, lb/in.
R_c	axial-stress ratio
R_s	shear-stress ratio
r	shear-stiffness parameter for sandwich plate
r_w	bend radius, in.
$s = \left(D_c/D_t\right)^{1/2}$	
t	thickness of plate, in.
t_f	thickness of sandwich facings, in.
$\bar{t}$	effective thickness, in.
u,v,w	displacements, in.

W
1
2
2

w	total width of compression cover, in.
x,y,z	coordinates
α_s	efficiency coefficient of shear webs
β	crippling coefficient
β_r	crippling coefficient of riveted multiweb beam
γ	stiffener-rigidity parameter, EI/bD
ϵ	strain
ϵ_e	edge strain
η	plasticity-reduction factor
$\bar{\eta}$	effective plasticity-reduction factor
ν	Poisson's ratio
ν_e	elastic Poisson's ratio
Σ	solidity
σ	normal stress, psi
σ_{cr}	buckling stress, psi
σ_{cy}	compressive yield strength, psi
$\bar{\sigma}_f$	crippling strength, psi
$\bar{\sigma}_{fr}$	strength of riveted multiweb beam, psi
τ	shear stress, psi
τ_y	shear yield strength, psi
$\bar{\tau}$	plasticity-reduction factor for wide columns
$\bar{\tau}_o$	effective optimum shear stress, psi
Υ	post-stiffness parameter, $Kb_s^3/\pi^4 D_c L_t$

φ	density, lb/cu in.
$\bar{\varphi}$	density of core, lb/cu in.

Subscripts:

c	compression cover or core
cr	buckling
cy	compressive yield
e	effective or edge
f	failure or facings
o	optimum
p	post
s	plate or shear
t	tension cover
w	web
x,y	coordinates

W
1
2
2

ORTHOTROPIC-PLATE THEORY

Stiffening-System Classification

The load-carrying capacity of a flat plate is frequently increased by the application of stiffeners to the plate. These may serve to carry load, to stiffen the plate so as to increase its buckling stress, or both. The stiffeners usually are discrete elements fastened to the plate at regular intervals or fabricated as part of a monolithic structure. This latter type is often referred to as integral construction and represents the ultimate in fastening efficiency.

It is pertinent, at this point, to review the classification for stiffened plates as discussed in reference 2. Two major factors in the classification are the number of skins employed and the type of stiffening system used to support the skins.

Single-skin construction includes longitudinal-, transverse-, and waffle-grid-stiffened plates. Double-skin construction is essentially a sandwich with various types of cores such as honeycomb or corrugations. Representative stiffening systems for single-skin plates are shown in figure 1 which pictures integral plates with longitudinal, transverse, and waffle-grid stiffening. Under certain conditions presented in the following discussion, these forms of construction may be considered as orthotropic plates.

Orthotropic Behavior

An orthotropic structure has mechanical properties that are constant throughout the structure but are different in different directions. Few engineering structures are uniformly orthotropic; however, under certain conditions they may be analyzed on the assumption of orthotropicity. Some representative cases are discussed in this section in regard to buckling of stiffened plates.

A rectangular flat plate may be stiffened by the addition of members attached to the plate at any angle to the sides. These stiffeners usually are discrete structural members which support the plate normal to its plane. They may also provide some rotational restraint to the plate along the lines of attachment of the stiffeners. The stiffeners can also assist in carrying the load applied to the plate, as is the case with longitudinally stiffened plates loaded in longitudinal compression.

Consider the effect of adding transverse stiffeners to a longitudinally compressed plate. Assume that the stiffener rigidity is less than that required to enforce a transverse node in the plate when it buckles. The buckling behavior of such a plate is shown in figure 2(a), in which the effect of transverse stiffeners upon the buckling performance of the plate may be seen. It is apparent from the figure that the plate behaves almost as if it were orthotropic when $n = 3$. This behavior pattern is also expected of longitudinally stiffened plates under longitudinal compression, as evidenced by the charts in figure 10 of Part II of this Handbook (ref. 3). Figures 10(a) to 10(i) present data for one, two, and three stiffeners while figures 10(j) to 10(l) contain information for an infinite number. Little difference exists among the curves for $n = 3$ and $n = \infty$, except for values of EI/bD approaching 0.

Orthotropic buckling theory is in excellent agreement with that for a single longitudinal stiffener on a rectangular flat plate loaded in shear as may be seen in figure 2(b). However, data for transversely stiffened plates in shear indicate that orthotropic theory is not applicable except where the stiffness ratio EI/bD is very small or very

large (fig. 2(c)). There is a range of values of EI/bD in which orthotropic theory predicts buckling stresses that differ widely from the theory for discrete stiffeners and from test data which agree with the discrete theory within reasonable limits of error. Part of the discrepancy may possibly be due to the neglect of certain buckling modes from the orthotropic analysis.

To summarize, then, orthotropic theory may be used for compressed plates with three or more stiffeners, for plates in shear with any number of longitudinal stiffeners, and for transversely stiffened plates in shear for relatively small or large values of EI/bD.

Load-Deformation Relations

In deriving either the differential equation for equilibrium of a plate element or the energy integrals it is necessary to proceed from the basic load-deformation relationships. The assumptions made in deriving the isotropic plate equations in the elastic range are that Hooke's law applies, that deflections of the plate normal to its originally flat configuration are small compared with the plate thickness, and that plane sections before bending remain plane after bending. Then, since stress will be proportional to the distance from the neutral surface, Hooke's law may be written (ref. 4):

$$\left.\begin{aligned}
\sigma_x &= -\frac{Ez}{1 - \nu_e^2}\left(\frac{\partial^2 w}{\partial x^2} + \nu_e \frac{\partial^2 w}{\partial y^2}\right) \\
\sigma_y &= -\frac{Ez}{1 - \nu_e^2}\left(\frac{\partial^2 w}{\partial y^2} + \nu_e \frac{\partial^2 w}{\partial x^2}\right) \\
\tau &= -2Gz \frac{\partial^2 w}{\partial x\, \partial y}
\end{aligned}\right\} \tag{1}$$

When these equations for stress are integrated across the plate thickness, relations are obtained between moment and curvature in the form

$$\left.\begin{aligned}
M_x &= -D\left(\frac{\partial^2 w}{\partial x^2} + \nu_e \frac{\partial^2 w}{\partial y^2}\right) \\
M_y &= -D\left(\frac{\partial^2 w}{\partial y^2} + \nu_e \frac{\partial^2 w}{\partial x^2}\right) \\
M_{xy} &= M_{yx} = -D\left(1 - \nu_e\right)\frac{\partial^2 w}{\partial x\, \partial y}
\end{aligned}\right\} \tag{2}$$

The coefficient of the bending-curvature terms is the plate rigidity in bending and is defined as

$$D = Et^3/12\left(1 - \nu_e^2\right) \tag{3}$$

The twisting rigidity for the isotropic plate is equal to $\left(1 - \nu_e\right)D$.

For an orthotropic plate, Hooke's law becomes

$$\left.\begin{aligned}
\sigma_x &= -\frac{z}{1 - \nu_x\nu_y}\left(E_x \frac{\partial^2 w}{\partial x^2} + E' \frac{\partial^2 w}{\partial y^2}\right) \\
\sigma_y &= -\frac{z}{1 - \nu_x\nu_y}\left(E_y \frac{\partial^2 w}{\partial y^2} + E' \frac{\partial^2 w}{\partial y^2}\right) \\
\tau &= -2Gz \frac{\partial^2 w}{\partial x\, \partial y}
\end{aligned}\right\} \tag{4}$$

in which use is made of the reciprocal relation

$$E_x\nu_y = E_y\nu_x = E' \tag{5}$$

The moment-curvature relations then become, upon integration of equations (4) across the plate thickness,

$$\left.\begin{aligned}
M_x &= -D_x \frac{\partial^2 w}{\partial x^2} - D' \frac{\partial^2 w}{\partial y^2} \\
M_y &= -D_y \frac{\partial^2 w}{\partial y^2} - D' \frac{\partial^2 w}{\partial x^2} \\
M_{xy} &= -2D_{xy} \frac{\partial^2 w}{\partial x\, \partial y}
\end{aligned}\right\} \tag{6}$$

where

$$\left.\begin{aligned} D_x &= \frac{E_x t^3}{12\left(1 - \nu_x \nu_y\right)} \\ D_y &= \frac{E_y t^3}{12\left(1 - \nu_y \nu_x\right)} \\ D' &= \frac{E' t^3}{12\left(1 - \nu_x \nu_y\right)} \\ D_{xy} &= \frac{G t^3}{12} \end{aligned}\right\} \tag{7}$$

W
1
2
2

Equations (6) neglect shear deformation and coupling. The former could exist in isotropic plates but may be relatively insignificant. However, in a sandwich, local shear deflections could be significant, as shown by Libove and Batdorf (ref. 5), for example.

In isotropic plates, or in plates for which geometrical symmetry exists, structural coupling is not to be expected. However, in a waffle grid, for example, the N_x forces may have a centroid different from that of the N_y forces. Coupling would occur through the resultant Poisson ratio effects which could lead to curvatures of the plate.

In general, the coupling terms can be found by first generalizing equations (6) to include membrane forces by writing the expressions for curvature and strain in terms of the internal forces and moments. These equations are:

$$\left.\begin{aligned} \frac{\partial^2 w}{\partial x^2} &= c_{11}M_x + c_{12}M_y + c_{13}M_{xy} + c_{14}N_x + c_{15}N_y + c_{16}N_{xy} \\ \frac{\partial^2 w}{\partial y^2} &= c_{21}M_x + c_{22}M_y + c_{23}M_{xy} + c_{24}N_x + c_{25}N_y + c_{26}N_{xy} \\ \frac{\partial^2 w}{\partial x\,\partial y} &= c_{31}M_x + c_{32}M_y + c_{33}M_{xy} + c_{34}N_x + c_{35}N_y + c_{36}N_{xy} \\ \frac{\partial u}{\partial x} &= c_{41}M_x + c_{42}M_y + c_{43}M_{xy} + c_{44}N_x + c_{45}N_y + c_{46}N_{xy} \\ \frac{\partial v}{\partial y} &= c_{51}M_x + c_{52}M_y + c_{53}M_{xy} + c_{54}N_x + c_{55}N_y + c_{56}N_{xy} \\ \frac{\partial u}{\partial y} + \frac{\partial v}{\partial x} &= c_{61}M_x + c_{62}M_y + c_{63}M_{xy} + c_{64}N_x + c_{65}N_y + c_{66}N_{xy} \end{aligned}\right\} \tag{8}$$

These relations omit the effects of transverse shear forces Q_x and Q_y.

From symmetry considerations $c_{ij} = c_{ji}$ and the 36 flexibility coefficients are reduced to 21. The curvature relations become

$$\left.\begin{aligned}
\frac{\partial^2 w}{\partial x^2} &= c_{11}M_x + c_{12}M_y + c_{13}M_{xy} + c_{14}N_x + c_{15}N_y + c_{16}N_{xy} \\
\frac{\partial^2 w}{\partial y^2} &= c_{12}M_x + c_{22}M_y + c_{23}M_{xy} + c_{24}N_x + c_{25}N_y + c_{26}N_{xy} \\
\frac{\partial^2 w}{\partial x\,\partial y} &= c_{13}M_x + c_{23}M_y + c_{33}M_{xy} + c_{34}N_x + c_{35}N_y + c_{36}N_{xy}
\end{aligned}\right\} \qquad (9)$$

The terms outside the boxes correspond to the usual isotropic quantities as expressed in equations (6), while the remaining terms are what are referred to by Libove and Hubka as "coupling terms" (ref. 6). Actually, in their development of orthotropic-plate theory, it was assumed that

$$c_{13} = c_{16} = c_{23} = c_{26} = c_{34} = c_{35} = 0$$

Thus, the orthotropic-plate relations between internal forces and deformations become

$$\left.\begin{aligned}
\frac{\partial^2 w}{\partial x^2} &= c_{11}M_x + c_{12}M_y + c_{14}N_x + c_{15}N_y \\
\frac{\partial^2 w}{\partial y^2} &= c_{12}M_x + c_{22}M_y + c_{24}N_x + c_{25}N_y \\
\frac{\partial^2 w}{\partial x\,\partial y} &= c_{13}M_{xy} + c_{36}N_{xy} \\
\frac{\partial u}{\partial x} &= c_{14}M_x + c_{24}M_y + c_{44}N_x + c_{45}N_y \\
\frac{\partial v}{\partial y} &= c_{15}M_x + c_{25}M_y + c_{45}N_x + c_{55}N_y \\
\frac{\partial u}{\partial y} + \frac{\partial v}{\partial x} &= c_{63}M_{xy} + c_{66}N_{xy}
\end{aligned}\right\} \qquad (10)$$

The c_{ij} are plate flexibilities. The rigidities are obtained by inverting equations (10) so that the forces and moments are expressed in terms of the strains and curvatures. For details concerning derivation of the coefficients, reference 6 should be consulted.

Effectively, coupling may be described as the generation of one type of deformation by a loading of a different type. For example, bending moments not only give rise to curvature but also couple into axial deformation, and axial forces couple into curvature. The latter may be seen by referring to the transversely stiffened plate in figure 1. Compressive forces acting in the longitudinal direction would tend to expand the plating in the transverse direction by the Poisson ratio effect. Since this growth would take place in a plane displaced from that containing the neutral axis of the cross section normal to the transverse direction, a curvature $\partial^2 w/\partial y^2$ and bending moments M_y would be generated in the plate.

Equilibrium Equations

The analysis of orthotropic-plate buckling problems may involve the use of either the equilibrium differential equation or the energy method. This section contains a brief description of the derivation of the equilibrium equation with the purpose of highlighting the differences between the isotropic and orthotropic theories.

The equilibrium equation in terms of the internal moments is (ref. 4):

$$\frac{\partial^2 M_x}{\partial x^2} - 2\frac{\partial^2 M_{xy}}{\partial x\,\partial y} + \frac{\partial^2 M_y}{\partial y^2} + p = 0 \tag{11}$$

When the isotropic moment-curvature relations are inserted into equation (11) the equilibrium equation is

$$D\nabla^4 w = p \tag{12}$$

The membrane forces may be added to obtain

$$D\nabla^4 w + \bar{t}\left(\sigma_x \frac{\partial^2 w}{\partial x^2} + 2\tau \frac{\partial^2 w}{\partial x\,\partial y} + \sigma_y \frac{\partial^2 w}{\partial y^2}\right) = p \tag{13}$$

The orthotropic equilibrium equation becomes from equation (11)

$$D_x \frac{\partial^4 w}{\partial x^4} + 2\left(D' + 2D_{xy}\right)\frac{\partial^4 w}{\partial x^2 \partial y^2} + D_y \frac{\partial^4 w}{\partial x^4} = p \tag{14}$$

or the membrane forces may be added to obtain

W
1
2
2

$$D_x \frac{\partial^4 w}{\partial x^4} + 2\left(D' + 2D_{xy}\right)\frac{\partial^4 w}{\partial x^2 \partial y^2} + D_y \frac{\partial^4 w}{\partial y^4} + \bar{t}\left(\sigma_x \frac{\partial^2 w}{\partial x^2} + 2\tau \frac{\partial^2 w}{\partial x\, \partial y} + \sigma_y \frac{\partial^2 w}{\partial y^2}\right) = p \tag{15}$$

A more generalized derivation of the orthotropic equilibrium equation was performed by Libove and Batdorf (ref. 5) for sandwich plates. The following equation pertains to an isotropic plate with finite shear rigidity:

$$D\nabla^4 w + \bar{t}\left(1 - \frac{D}{\bar{C}}\nabla^2\right)\left(\sigma_x \frac{\partial^2 w}{\partial x^2} + 2\tau \frac{\partial^2 w}{\partial x\, \partial y} + \sigma_y \frac{\partial^2 w}{\partial y^2}\right) = p \tag{16}$$

Elastic Constants

The bending and axial rigidities of a plate may be determined either theoretically or experimentally. For a simple structure such as an isotropic plate it is a simple matter to calculate the plate rigidities. However, for a waffle-grid plate, or for a plate stiffened by riveted members, it may be difficult to compute rigidities accurately, particularly when coupling is significant. In such cases it is necessary to utilize experimental procedures. Riveted connections involve flexibilities between the stiffener and plate which may vary with the method of riveting although the plate and stiffener designs do not change. Consequently, rigidities for this type of construction would be most reliably determined experimentally.

A sandwich plate with a cellular or honeycomb core would be symmetrical about its midplane and consequently no coupling would be present. However, the behavior of a sandwich is dependent upon the shear rigidity of the core, which may be determined by separate tests of the core material. The analysis of corrugated-core sandwiches may involve coupling if the corrugations are not symmetric about the plate midplane.

In the following section the elastic constants of each of these types of construction are discussed in some detail from the standpoint of their application in plate buckling problems.

STABILITY OF ORTHOTROPIC FLAT PLATES

General Solutions

Most orthotropic-plate buckling problems have implicit solutions which require the use of design curves. Some explicit solutions which have rather wide application have appeared in the literature, however. Wittrick investigated simply supported flat plates under uniaxial and biaxial compression (ref. 7), while the flat-plate limit of Hayashi's solution to torsional buckling of orthotropic cylinders (ref. 8) pertains to long orthotropic plates under shear. Seydel analyzed finite-length plates in shear (ref. 9). These three cases are discussed below.

Compressive buckling.- Wittrick analyzed a simply supported flat orthotropic plate under forces N_x and N_y using, as an expression for w in equation (15),

$$w = w_o \sin(m\pi x/a)\sin(n\pi y/b) \tag{17}$$

He found that the solution to the problem may be written in the form

$$k = \left[\frac{(a/b)_e}{m} + \frac{m}{(a/b)_e}\right]^2 \tag{18}$$

where

$$k = 2 + \frac{\left(b^2N_x/\pi^2\right) - 2D_{xy}}{\left\{\left(D_yD_x\right)\left[1 - \left(b^2N_y/\pi^2D_y\right)\right]\right\}^{1/2}} \tag{19}$$

and

$$(a/b)_e = (a/b)\left\{\left(D_y/D_x\right)\left[1 - \left(b^2N_y/\pi^2D_y\right)\right]\right\}^{1/4} \tag{20}$$

For uniaxial compression $N_y = 0$ and equation (19) reduces to

$$k = \left(\frac{b}{\pi}\right)^2 \frac{N_x}{\left(D_x D_y\right)^{1/2}} + C\left[1 - \frac{D_{xy}}{\left(D_x D_y\right)^{1/2}}\right] \tag{21}$$

The coefficient C in equation (21) depends upon the boundary conditions as follows:

Boundary conditions	C
All edges simply supported	2
Loaded edges clamped, unloaded edges simply supported	2
Loaded edges simply supported, unloaded edges clamped	2.40
All edges clamped	2.46

Wittrick found that isotropic-plate buckling coefficients may be used for orthotropic plates provided that the effective aspect ratio for the latter, equation (20), is used to evaluate k. The curves in figure 3 as taken from Part I of this Handbook (ref. 10) are included herein for use with orthotropic plates.

Two cases of biaxial compression may also be analyzed by using figure 3. These cases are of plates with two edges simply supported and the other two edges either simply supported or clamped. The value of $(a/b)_e$ from equation (20) is found in the figure and the value of k is found from the appropriate curve. Equation (19) is then used to complete the analysis.

Shear buckling.- The shear buckling of orthotropic plates was investigated by Seydel (ref. 9) and the theoretical critical loading was obtained in the form

$$N_{xy_{cr}} = \frac{k_s \pi^2 \left(D_x D_y^3\right)^{1/4}}{b^2} \tag{22}$$

in which k_s is dependent upon the effective aspect ratio $(a/b)_e$ and the parameter $\bar{c} = D_{xy}\left(D_x D_y\right)^{-1/2}$. Values of k_s may be found in figure 4(a) for plates with all edges simply supported and in figure 4(b) for plates with clamped short edges and simply supported long edges. Figure 4(b) was obtained from reference 4.

The analysis performed by Hayashi on stiffened circular cylinders in torsion (ref. 8) approaches a long plate in shear as a limiting case. The resultant expression for the shear-buckling load of an infinitely long, simply supported, orthotropic plate is

$$N_{xy_{cr}} = \frac{5.35\pi^2 D_x}{b^2} \tag{23}$$

By making use of the relation

$$\nu_y D_x = \nu_x D_y$$

equation (22) can be transformed into

$$N_{xy_{cr}} = \frac{k_s \pi^2 D_x}{b^2}\left(\frac{\nu_y}{\nu_x}\right)^{3/4} \tag{24}$$

This equation differs from equation (23) in the Poisson ratio term and in the dependence of k_s upon $\bar{c}$. For a long isotropic plate these two results are identical since $\nu_x = \nu_y = \nu$ and k_s assumes a value of 5.35.

Transverse compression and shear.- Sandorff investigated the stability of a transversely stiffened plate under combined transverse compression and shear loading (ref. 11). The stiffeners were numerous and closely spaced, and consequently orthotropic theory was used. The energy method was applied with an assumed double-sine-series deflection function which corresponds to simply supported edges. The analysis was simplified by assuming the panel to be infinitely wide. The interaction data appear in figure 5.

The theory predicted an interaction curve of the same shape as that for an isotropic plate under the same combined loading. Test data from a box beam in combined bending and torsion were compared with the theory. The agreement is good although the actual dimensions of the panel in the box beam yield $a/b = 1/2$. However, Sandorff determined that the effective aspect ratio to be used in this orthotropic theory is $(a/b)(E_y I_y/E_x I_x)$, which has a value of 1/3,800 for the test panel. Consequently, the assumption of an infinitely wide column would be justified.

Sandwich plates.- The buckling analysis of simply supported sandwich plates was performed by Seide and Stowell in the elastic and inelastic ranges (ref. 12). The differential equation for the elastic case obtained from equation (16) is

$$D_s\nabla^4 w + \left(1 - \frac{D_s}{h_c G_c}\nabla^2\right)2\sigma_c t_f \frac{\partial^2 w}{\partial x^2} = 0 \tag{25}$$

Equation (25) contains the correction term $D_s/h_c G_c$, in which the shearing rigidity of the core $h_c G_c$ appears. In an isotropic plate, G_c is assumed to be infinite. However, in a sandwich such an assumption may lead to significant errors in the buckling stress. The section properties of a non-load-carrying-core sandwich are such that $\nu_x = \nu_y = \nu_f$ for the faces and

$$D_x = D_y = \left(1 + \nu_f\right)D_{xy} = D_s = \frac{E_f t_f h_c^2}{2\left(1 - \nu_f^2\right)} \tag{26}$$

This type of plate is referred to as an isotropic sandwich plate.

Seide and Stowell found the buckling-stress coefficient to be, before minimization,

$$k = \frac{2b^2\sigma_{cr}t_f}{\pi^2 D_s} = \frac{\left(\frac{a}{mb} + \frac{mb}{a}\right)^2}{1 + r\left[1 + \left(\frac{mb}{a}\right)^2\right]} \tag{27}$$

in which r is the core shear stiffness parameter for the sandwich and

$$r = \frac{\pi^2 D_s}{b^2 h_c G_c} \tag{28}$$

The expression for k in terms of ma/b is the same as that for an isotropic plate except for the denominator correction $r\left[1 + (mb/a)^2\right]$. For infinite values of G_c this will vanish, yielding the isotropic result.

The solution to the sandwich plate-buckling problem is obtained by minimization of equation (27) with respect to a/mb. Two ranges are found for the solution: for $r \leq 1$

$$\left.\begin{aligned} a/mb &= \left[(1 - r)/(1 + r)\right]^{1/2} \\ k &= 4(1 + r)^{-2} \end{aligned}\right\} \tag{29}$$

and for $r \geqq 1$

$$\left.\begin{aligned} a/mb &= 0 \\ k &= 1/r \end{aligned}\right\} \tag{30}$$

Equations (29) reduce to $a/mb = 1$ and $k = 4$ for the isotropic case.

W
1
2
2

Design charts are described in a subsequent section on sandwich plates in which data are presented for specific types of cores. The curve of k as a function of r for long plates appears in figure 6 for the practical design range in which $r \leqq 1$.

Seide computed compressive buckling stresses for isotropic sandwich plates with simply supported loaded edges and clamped unloaded edges (ref. 13). For $r \geqq 0.5$ the buckling-coefficient curve for a long plate merges with that for a simply supported plate as seen in figure 6.

Seide also analyzed buckling of an infinitely long simply supported isotropic plate in shear (ref. 14). The curve of k_s as a function of r appears in figure 6(b). The energy method was used for that investigation in which a Fourier analysis was employed.

Single-Skin Systems

The general orthotropic plate-buckling solutions presented in figures 3 to 6 are given in terms of certain plate rigidities. For application to specific forms of construction, it is necessary to evaluate the pertinent rigidity terms. Consequently, the remainder of this section is devoted to a review of theoretical and experimental methods of evaluating the elastic constants of single- and double-skin forms of construction as well as of methods of determining buckling stresses.

Longitudinally stiffened plates.- Theoretical-buckling-stress data for longitudinally compressed longitudinally stiffened plates are presented in Part II of this "Handbook of Structural Stability" (ref. 3). Charts are included for one-, two-, and three-stiffener systems and for an infinite number of stiffeners. In addition, theoretical corrections are included for the effects of one-sided stiffening. The information was obtained from the reports of Seide and Stein (refs. 15 and 16) which

should be consulted for details. The structural rigidities for these analyses were computed from the geometries of the stiffened plate sections.

Shear buckling of longitudinally stiffened plates was discussed in the section "Orthotropic-Plate Theory" of the present paper. Theoretical and experimental data appear in figure 19(a) of reference 3.

Transversely stiffened plates.- Longitudinal compressive-buckling coefficients of simply supported transversely stiffened plates are presented in figure 13 of reference 3. The stiffener spacing is small in all cases, with a maximum aspect ratio of 0.5 for the plate between stiffeners. The effect of finite stiffener torsional rigidity is included on these charts. Rigidities were computed from the section properties.

The minimum weight design of transversely stiffened plates in longitudinal compression was investigated by Gerard (ref. 17) and by Gomza and Seide (ref. 18). Gomza and Seide derived relations for nondimensional parameters of the problem and minimized them to obtain equations which were used to prepare design charts. These charts yielded combinations of the plate parameters for minimum weight under the applied loading. However, all the combinations are implicit relations. Total weight, or weight of the stiffening structure, is not directly available from these charts.

It is possible to simplify the presentation of Gomza and Seide to obtain more general optimum design information. Gerard minimized the section solidity to demonstrate that the optimum stiffener weight should be one-third that of the plate, that the stiffeners should be closely spaced, and that the weight would be large in the practical loading range. For detailed discussions of the assumptions made in these investigations, a review of references 11 and 12 is recommended.

Buckling-stress information for simply supported transversely stiffened plates in shear appears in figure 19(b) of reference 3. This problem was discussed previously in the section "Orthotropic Plate Theory" of the present report.

Waffle-grid plates.- When rectangular plates under longitudinal compression are considered, longitudinal and transverse stiffeners represent the extremes of possible stiffening configurations for which the direction of stiffening is permitted to vary between the limits of 0° (parallel to the long side of the rectangle, in which direction the load is applied) and 90° (parallel to the short side of the rectangle and transverse to the loading). The term "waffle grid" has been applied to such a plate because of the appearance of the stiffening system in which the stiffeners are arranged symmetrically on the plate.

Theoretical and experimental investigations were performed by the NACA on integral waffle-grid construction. The results are summarized in the report by Dow, Levin, and Troutman (ref. 19) who conducted tests on square tubes, each face of which was a waffle-grid plate. One tube was used for each grid configuration. The specimens were cast from 355 aluminum alloy and were then heat-treated to the T61 condition. They were loaded in longitudinal compression, in shear, and in combinations of these loads in various proportions. The plates were clamped on the short edges and were simply supported on the long edges.

Nine waffle-grid configurations were tested, and the results were compared with theoretical results. Good agreement was obtained both in the elastic and inelastic ranges for both types of loading. The theories with which the data were compared are those of Wittrick for compression and Seydel for shear. They were discussed previously in the section on general solutions. The elastic constants used by Dow, Levin, and Troutman in applying the theories to analysis of the waffle grids were obtained from the report by Dow, Libove, and Hubka (ref. 20) in which both experimental and theoretical procedures are described. Good agreement was obtained in some cases, and appreciable discrepancies in others. In general, it appears advisable to obtain rigidities experimentally.

An electric-analog investigation of torsional rigidity for filleted integral ribs was performed by Crawford and Libove (ref. 21) for a large range of rib and fillet proportions. However, no interaction with neighboring structures was considered and consequently the effect of resistance to warping was not evaluated.

One result of the investigation of Dow, Levin, and Troutman (ref. 19) was the indication that a stiffening system at 45° (so-called ±45° stiffening) carried the largest compressive load of the types of grids tested, all of which were approximately the same weight. In shear the ±60° grid was theoretically the best under elastic buckling. However, in inelastic buckling the ±45° and ±60° waffle-grid plates were equally efficient.

Inelastic buckling stress was computed using the secant-modulus method both for compression and shear loading. It is interesting to note that the maximum discrepancy between theory and experiment was 22 percent in the elastic range while in the inelastic range it was 5 percent.

A calculation was made of the theoretical critical loading on one of the 0°-grid plates using the data in Part II of the Handbook (ref. 3) for longitudinally stiffened plates. The loading found in this manner was 8 percent above the experimental value, which in turn was 12 percent higher than the value from Wittrick's theory. Both theories are predicated upon the assumption that the stiffener axis lies in the midplane of the plate. The off-axis correction was not employed in this computation.

Crawford (ref. 22) demonstrated that the buckling load of a plate with one side stiffened is essentially that of the same plate with a central-plane stiffener. The results for the waffle-grid plates would appear to bear this out. Crawford analyzed this problem employing large-deflection theory which involved the effect of structural coupling. He applied the theory to the analysis of the elastic behavior of a simply supported square plate under uniaxial compression. The theory predicted that the plate with the one-sided stiffening system would deflect normal to its plane immediately upon application of load, and that these deflections would grow as the load increased. This is much the same action as an initially imperfect column or plate. The limiting load which the plate appeared to approach asymptotically was the buckling load of the symmetrically stiffened plate of the same stiffness. The implication in this result, which is substantiated by the waffle-grid test data, is that the buckling stress of the plate considered was relatively unaffected by coupling action.

Dow, Levin, and Troutman (ref. 19) compared the data obtained from combined longitudinal compression and shear loadings with an interaction curve of the form

$$R_c + R_s^2 = 1 \tag{31}$$

Presumably, more test data will be required before an appropriate interaction equation can be selected for this loading combination applied to waffle-grid plates, since the scatter of the data was too large to permit drawing a conclusion concerning the reliability of equation (31).

Double-Skin Systems

A double-skin, or sandwich system consists of two thin plates joined together by a core structure. Such a system is divisible into two classifications according to the load-carrying ability of the core as compared with that of the covers.

When the core rigidity is such that $t_cE_c \ll 2t_fE_f$, the core is assumed to be non-load-carrying. This class would include end-grain woods (balsa particularly), foam structures, and cellular cores. When $t_cE_c \rightarrow 2t_fE_f$ for any direction of load applied in the plane of the plate, the core is considered to be load carrying in that direction. This class would include corrugated and truss cores. In this section, plates are discussed under these two classifications.

A detailed development of equilibrium differential equations and energy integrals for sandwich plates was presented by Libove and Batdorf

(ref. 5). Solutions to these equations have been obtained for certain specific cases, some of which are discussed herein. In addition, optimum sandwich-plate designs have been developed. A comprehensive treatment of sandwich construction is contained in reference 23 in which data on buckling of sandwich plates may be found. In this section, discussions are limited to brief reviews of some of this information, together with a summary of pertinent data on optimum design.

Non-load-carrying cores.- The analysis of uniaxial compressive buckling of isotropic sandwich plates was discussed in the section on general solutions. Johnson and Semonian (ref. 24) investigated honeycomb- W
core sandwich plates under uniaxial compression by utilizing the solution 1
of Seide and Stowell (ref. 12). In order to apply the theory it was nec- 2
essary to evaluate the shear stiffness parameter r defined in equa- 2
tion (28). When this was done the axial load-carrying capacity of the plate was determined in terms of the core and facing dimensions and material properties. Johnson and Semonian provided design charts for steel sandwich plates at 80° and 600° F. The data pertain to plates of optimum proportions determined according to a report by Bijlaard (ref. 25).

Experimental data obtained by Anderson and Updegraff (ref. 26) were compared with theory for $0.02 < r < 0.8$. The agreement was found to be good except for a few test specimens which buckled at a stress below the predicted value. Anderson and Updegraff suggest that this was due to the low shear strengths of the cores in these specimens.

Charts of buckling-stress coefficients for various types of loading and plate proportions appear in reference 23. The use of these charts requires a knowledge of the elastic constants of the sandwich plate. Johnson and Semonian computed the shear flexibility parameter r from the plate cross-section geometry (ref. 24). This is the general practice for isotropic sandwich plates since the symmetrical construction eliminates coupling, thereby presumably obviating experimental determination of the elastic constants that enter the relation for the r shown in equation (28).

The optimum design of an isotropic sandwich plate subject to instability was investigated by Bijlaard (ref. 25) and by Gerard (refs. 2 and 17). Results from reference 17 indicate that for elastic buckling of a simply supported isotropic sandwich plate under uniaxial compression the optimum distribution of material is obtained when the core weight is twice that of the covers. Furthermore, for a core relatively stiff in compression normal to the plate faces, the optimum thickness ratio of the core and covers is

$$\left(h/2t_s\right)_o = 2\varphi/\overline{\varphi} \tag{32}$$

When the facings of a uniaxially compressed simply supported sandwich plate are designed to operate at the compressive yield strength no simple generalizations such as those for the elastic case are possible. Procedures and charts for yield-strength design are contained in references 2 and 24.

Load-carrying cores.- Data on buckling of orthotropic sandwich plates, which include corrugated core construction, appear in reference 23. Libove and Hubka evaluated elastic constants of various shapes of corrugations including those unsymmetrical about the plate midplane in reference 6. These were also evaluated experimentally by a procedure described in that report in considerable detail. It follows the general experimental procedure outlined by Libove and Batdorf in reference 5.

Seide (ref. 27) analyzed buckling of sandwich plates under longitudinal compression with simply supported loaded edges and either simply supported or clamped unloaded edges. The investigation was restricted to flat symmetric corrugations. The constants derived by Libove and Hubka were used in this analysis. Seide's report should be consulted for design data.

Corrugated-core plates have little shear rigidity in a plane normal to the plate covers and parallel to the corrugations. The use of a truss corrugation would add stiffness in this direction. Anderson and Updegraff (ref. 26) reported theoretical data for the design of such a system. The buckling stress for transverse compression was found to be roughly half that for longitudinal compression. A design chart is included in reference 6 for an efficient high-strength steel structure.

BUCKLING AND FAILURE OF MULTIWEB BEAMS IN BENDING

The various preceding parts of this "Handbook of Structural Stability" have been concerned, for the most part, with buckling and failure of individual elements. Certain general instability considerations for box beams of stiffened panel-rib construction were presented in Part V (ref. 1), although the analysis did not treat the box beam as a unit in complete detail.

A competing form of box construction is the multiweb beam which has efficient application in the highly loaded, thin wings of supersonic aircraft. Because of the relative simplicity of this form of construction, however, it has been possible to treat buckling and failure of multiweb box beams in rather complete detail instead of considering individual components. Such analyses of the complete multiweb box are reviewed in this section.

The buckling and failure modes under bending of representative multiweb box beams shown in figure 7 can be divided into the following areas:

(a) Local instability of the cover in compression between webs

(b) Local instability of the webs in bending

(c) Crushing of the webs by the transverse compressive component of the cover loads

(d) Wrinkling of the cover (as a wide column) over the webs because of insufficient deflectional and rotational stiffness of the web-cover attachment

In addition to the various instability modes, it is advantageous to characterize various multiweb box beams according to the method of fabrication as follows:

(a) Integral forms of monolithic construction such as machined or extruded beams in which the web-cover attachment is in the plane of the web (fig. 7)

(b) Built-up construction in which the web generally consists of extruded or machined spar caps and sheet webs

(c) Formed channel-type webs (fig. 7)

The results presented in this section are in terms of stresses rather than bending moments. Although it is relatively simple to compute bending moments at buckling or failure of the simple rectangular box beams used in the tests reported herein, for airfoil sections of variable height it appears appropriate to present the results in terms of stresses.

Buckling Stresses

Anderson and Semonian (ref. 28) have presented a series of design charts which permit the evaluation of the compressive buckling stress of a long flat rectangular plate with various lengthwise deflectional and rotational elastic line supports. In order to use these charts to determine the compressive buckling stress of a multiweb-beam cover it is necessary to evaluate the deflectional and rotational restraints provided by the webs. Methods for evaluating these restraints are also discussed in reference 28.

These results constitute a general approach to the problem and are useful for a variety of web configurations. More specific results

in the form of buckling-coefficient charts which are essentially based on this approach are presented in the following discussion.

Integral webs.- Local buckling of the compression cover or webs of an integral type of multiweb box can be determined from the usual buckling-stress equation:

$$\sigma_{cr} = \frac{\pi^2 k\eta E}{12\left(1 - \nu_e^2\right)}\left(\frac{t_s}{b_s}\right)^2 \tag{33}$$

Schuette and McCulloch (ref. 29) have determined the values of k for a wide, idealized, integral multiweb box under bending and their results are shown in figure 8. These data incorporate the effects of the rotational restraints upon the buckling stress.

As a conservative approximation, Gerard (ref. 17) has considered a multiweb box beam with the web-cover attachment in the form of a hinge. In this case, there are no rotational restraints and the buckling coefficients are

$$\left.\begin{aligned} k &= 4 && \text{for } \frac{b_w/t_w}{b_s/t_s} \leqq 2.5 \\ k &= 25\left(\frac{b_s/t_s}{b_w/t_w}\right)^2 && \text{for } \frac{b_w/t_w}{b_s/t_s} > 2.5 \end{aligned}\right\} \tag{34}$$

The appropriate plasticity-reduction factors for use in equation (33) apparently depend upon the element responsible for buckling. When the cover buckles first, the value of η given in Part I (ref. 10) is appropriate:

$$\eta_s = \frac{1 - \nu_e^2}{1 - \nu^2}\left(E_s/E\right)\left\{\frac{1}{2} + \frac{1}{4}\left[1 + \left(3E_t/E_s\right)\right]^{1/2}\right\} \tag{35}$$

When the web buckles first, as an approximation

$$\eta_w = \frac{1 - \nu_e^2}{1 - \nu^2}\left(E_s/E\right) \tag{36}$$

Should the cover and web buckle simultaneously, then as an approximation

$$\bar{\eta} = (\eta_s \eta_w)^{1/2} \tag{37}$$

or

$$\bar{\eta} = \frac{1 - \nu_e^2}{1 - \nu^2}(E_s/E)\left\{\frac{1}{2} + \frac{1}{4}\left[1 + (3E_t/E_s)\right]^{1/2}\right\}^{1/2} \tag{38}$$

W
1
2
2

Another form of instability possible in an integral multiweb box under bending is crushing instability of the webs due to the transverse compressive component of the cover loading. In this case the web acts as a wide column which buckles according to

$$(\sigma_{cr})_w = \frac{\pi^2 k_w \bar{\tau} E}{12\left(1 - \nu_e^2\right)}\left(\frac{t_w}{b_w}\right)^2 \tag{39}$$

where for boxes simply supported at web-cover attachment

$$k_w = 1$$

and for boxes clamped at web-cover attachment

$$k_w = 4$$

The plasticity-reduction factor in this case is given in Part I (ref. 10) as

$$\bar{\tau} = \frac{1 - \nu_e^2}{1 - \nu^2}(E_s/E)\frac{1}{4}\left[1 + (3E_t/E_s)\right] \tag{40}$$

Rosen (ref. 30) has considered this problem and gives the web stress σ_w in terms of the cover stress σ_s for a rectangular box with identical covers by the following equation:

$$\sigma_w = 2\sigma_s \frac{b_s t_s}{b_w t_w} \epsilon_e \tag{41}$$

where ϵ_e is the edge strain at the attachment line. If the cover has not buckled before web crushing occurs, then the edge strain $\epsilon_e = \sigma_s/E$ and equation (41) becomes

$$\sigma_w = 2 \frac{\sigma_s^2}{E} \frac{b_s t_s}{b_w t_w} \tag{42}$$

By equating equations (39) and (42), the critical cover stress for crushing instability of the webs is

$$\left(\sigma_{cr}\right)_s = \left[\frac{\pi^2 k_w \bar{\tau}}{24\left(1 - \nu_e^2\right)}\right]^{1/2} E\left(\frac{t_w}{b_w} \frac{t_s}{b_s}\right)^{1/2} \frac{t_w}{t_s} \tag{43}$$

The analysis for web crushing after the cover buckles is presented in the later portion of this section which is concerned with failure rather than with buckling.

As a practical measure, crushing of an unstiffened web can be readily corrected in cases where it is theoretically possible by the use of stiffeners attached to the webs.

Built-up webs.- The essential difference between the buckling of built-up and integral multiweb beams is due to the additional rotational restraint provided by the attachment members. In cases of built-up beams, the buckling stress can be determined by the methods presented in reference 28. Some additional data on specific forms of built-up multiweb construction are given by Eggwertz (ref. 31) in the form of buckling-coefficient charts.

The buckling modes generally encountered for built-up beams are of the local-buckling type. Crushing instability may be analyzed according to the methods presented for integral beams. The wrinkling type of instability encountered in formed-channel-web construction, such as considered in the following section, can generally be avoided by placing the line of fasteners as close to the plane of the web as possible.

Formed channel webs.- Multiweb beams utilizing formed channel webs such as those shown in figure 7 can experience local buckling of the

cover or web and crushing instability of the web. These modes of instability can be analyzed according to the methods presented for integral beams. In addition, a wrinkling form of instability is frequently observed for beams with formed channel webs in which the buckling mode is characterized by waves extending across the entire width of the beam without the formation of longitudinal nodes. This wrinkling mode has previously been discussed for stiffened panels in Part V (ref. 1).

Bijlaard and Johnston (ref. 32) and Semonian and Anderson (ref. 33) have established that wrinkling results from the low deflectional stiffness of the web attachment flange, a characteristic of formed channel webs. In addition, the wrinkling stress was found to be sensitive to such details of the fastening system as offset, pitch, and diameter. W 1 2 2

The wrinkling mode is similar to local buckling in that buckling and failure may not be coincident. Thus, it is necessary to consider wrinkling instability separately from wrinkling failure.

According to the analysis of Semonian and Anderson (ref. 33), the cover stress for wrinkling instability is given by

$$\sigma_{cr} = \frac{\pi^2 k \bar{\eta} E}{12\left(1 - \nu_e^2\right)}\left(\frac{t_s}{b_s}\right)^2 \tag{44}$$

where k may be determined from figure 9. It can be observed that wrinkling instability can occur prior to local buckling depending upon the parameters $\left(b_w/t_w\right)/\left(b_s/t_s\right)$ and f/b_w as shown in figure 9.

Since both the web and cover are involved in wrinkling instability, the plasticity-reduction factor suggested in reference 33 is

$$\bar{\eta} = \left(\bar{\tau}\eta_w\right)^{1/2} \tag{45}$$

The cover buckles as a wide column and therefore a value of $\bar{\tau}$ given by equation (40) is appropriate. Using this value in conjunction with the value of η_w given by equation (36), equation (45) becomes

$$\bar{\eta} = \frac{1 - \nu_e^2}{1 - \nu^2}\left(E_s/E\right)\left[\left(1/4\right) + \left(3E_t/4E_s\right)\right]^{1/2} \tag{46}$$

In order to determine the wrinkling-instability coefficient k from figure 9, it is necessary to determine the effective offset

distance f. This parameter is a complex function involving the rivet pitch, diameter, and actual offset and is apparently best evaluated according to special tests outlined in reference 34.

For the tests reported in reference 35, the rivet pitch-diameter ratio was 3, the bend radius was $4t_w$, and the actual offset distance was approximately $7t_w$ in all cases. It was found that the effective offset distance for these tests was adequately approximated by using the actual offset distance as shown in figure 10. The experimental and theoretical k values are also shown in figure 10 and it can be observed that reasonably good agreement exists.

Failure Strength

Integral and built-up webs.- In reference 30, Rosen presented data on failing stresses in the compression cover of one- and two-cell extruded box beams of the integral type as well as three-cell built-up beams consisting of extruded channel webs. These data were successfully correlated therein utilizing test data on V-groove plates under compression.

In the interest of maintaining a uniform approach to the crippling problem throughout this Handbook, the test data presented in reference 30 were also analyzed according to the methods presented in reference 1. For a long flat plate with edges free to warp, the following crippling formula applies

$$\bar{\sigma}_f/\sigma_{cy} = \beta\left[\frac{t_s}{b_s}\left(\frac{E}{\sigma_{cy}}\right)^{1/2}\right]^m \tag{47}$$

where

$$\beta = 1.42$$

$$m = 0.85$$

The test data of reference 30 are shown in figure 11 according to the parameters of equation (47) and in conjunction with the constants derived from V-groove-plate test data. It can be observed that the test data for one-, two-, and three-cell boxes are in excellent agreement with equation (47). Apparently the use of one to three cells has an insignificant effect on the failing stress. The only exceptions are the two test points representing crushing failures of the webs. In this

case, the edge stress at the attachment line is less than the compressive yield strength and therefore a failure stress less than that given by equation (47) occurs.

In order to avoid premature failure due to web crushing, web stiffeners may be utilized. In cases where the webs are unstiffened, it appears as a suitable approximation that, for $\sigma_s = \bar{\sigma}_f$ according to equation (47), $\epsilon_e = \epsilon_{cy}$ in equation (41). Therefore, equation (41) becomes

$$\sigma_w = 2\bar{\sigma}_f \frac{b_s t_s}{b_w t_w} \epsilon_{cy} \tag{48}$$

W122

where

$$\epsilon_{cy} = \left(\sigma_{cy}/E\right) + 0.002$$

To avoid premature failure due to web crushing, the buckling stress of the web given by equation (39) must be greater than the applied web stress of equation (48).

Although crushing of the webs tends to reduce the failing strength below that given by equation (47), there are other factors which tend to raise the strength of the beam. In particular, if the webs provide rotational restraints for the cover and raise the buckling coefficient of the cover significantly above a value of $k = 4$, then equation (47) may be conservative.

For the integral and built-up beams used by Eggwertz (ref. 35), the webs contributed significant rotational restraints for the covers. These data are shown in figure 11 and are grouped according to number of cells where $k = 5.35$ and 6.35. It can be observed that the data lie consistently above those of reference 30 where a k value of approximately 4 existed. The slope of the lines correlating these data conforms to $m = 0.85$ for equation (47) although the β values are greater than 1.42.

In addition to these data, an additional test point which represents a bending test on an extruded rectangular tube as given in reference 36 is shown in figure 11. A value of $k = 5.5$ was estimated for this tube in reference 36. The average failing stress was calculated from the data of this report by subtracting the bending moment carried by the webs in accordance with the procedure given in reference 30.

A quantitative explanation of the somewhat higher β values for the data of references 35 and 36 can be obtained from equation (17) of

reference 37. The latter indicates that the β associated with $k > 4$ may be estimated from that associated with $k = 4$ as follows:

$$\beta = 1.42(k/4)^{0.425} \tag{49}$$

The β values shown in figure 11 for the k groups of 5.35 and 6.35 were obtained by use of equation (49) and apparently correlate reasonably well with the test data of references 35 and 36.

In addition to the increase in strength associated with a value of k greater than 4, prevention of warping of the unloaded edges of the compression cover tends to increase $\bar{\sigma}_f$ over that for a plate free to warp. This effect was discussed at some length in reference 37. Design factors which tend to restrain warping are a continuous cover over a large number of cells or the use of relatively heavy spar caps in built-up webs. Should such conditions be encountered in design, the prediction of $\bar{\sigma}_f$ by equation (47) may be somewhat conservative, particularly for $\bar{\sigma}_f/\sigma_{cy} < 0.80$.

Formed channel webs.- The failure of formed channel multiweb box beams under bending generally occurs as a result of either the local buckling- or wrinkling-instability mode. Semonian and Anderson (ref. 33) have considered wrinkling failures in addition to wrinkling instability and give the following formula for the cover stress at wrinkling failure:

$$\bar{\sigma}_f = \frac{\pi^2 k_f \bar{\eta} E}{12\left(1 - \nu_e^2\right)}\left(\frac{t_s}{b_s}\right)^2 \tag{50}$$

where $\bar{\eta}$ is given by equation (46) and the wrinkling-failure coefficient is

$$k_f = \left\{\frac{\left(48/\pi^4\right)}{\left(\frac{b_w/t_w}{b_s/t_s}\right)^3\left(\frac{f}{b_w}\right)^3}\left[\frac{\left(3f/b_w\right) + 1}{\left(3f/b_w\right) + 4}\right]\right\}^{1/2} \tag{51}$$

Test data of reference 34 on wrinkling failures of formed channel multiweb beams are compared with this theory in figure 12. The actual offset distance used to correlate the wrinkling-instability data of figure 10 was also used here. It can be observed that excellent agreement exists between the theory and test data in this case where the rivet pitch-diameter ratio was 3.

Needham (ref. 38) has also analyzed the test data of reference 34 by assuming that the strength of a multiweb box beam in bending depends upon the crippling strength of the web-skin junction. The agreement between the test data of reference 34 and Needham's method of analysis was very good.

Pride (ref. 38) has indicated, however, that, although Needham's method is in good agreement with the test data of reference 34 in which certain riveting parameters were assigned special values, the method may underestimate or overestimate the strength of multiweb box beams with different riveting parameters. Pride cites the results of seven different tests where the values predicted by Needham's method deviate from experiment from -32 to 40 percent.

It is concluded that small variations in the offset distance as well as variations in rivet pitch produce significant changes in the strength of formed channel multiweb beams. Because of this sensitivity to the riveting parameters, it is necessary to investigate experimentally the strength of any formed channel multiweb beam which deviates from the riveting details of the beams tested in reference 34. This statement applies to Needham's method and the theory of Semonian and Anderson as well as to the method of analysis presented in the following discussion.

In reference 1, test data on failure of short stiffened panels due to both local buckling and wrinkling instability were presented in terms of common parameters. It appears desirable to attain the same objective for formed channel multiweb beams in order to determine, for example, if this type of beam when subject to local buckling attains the crippling strength of a comparable integral type of construction.

For this purpose, the revised wrinkling-failure analysis of reference 1 can be presented in the following form:

$$\bar{\sigma}_{fr}/\sigma_{cy} = \beta_r\left[\frac{t_s}{b_s}\left(\frac{E}{\sigma_{cy}}\right)^{1/2}\right]^m \tag{52}$$

where β_r is a function of F and $F = \left(f/t_w\right)\left(b_w/t_w\right)^{1/8}$. In this form, equation (52) depends upon the same parameters as does equation (47) for the crippling strength of an integral multiweb beam with the exception that β_r is a function of a riveting parameter.

The test data of reference 34 were correlated according to the parameters of equation (52) in figure 13. All data for the $t_w/t_s = 0.37$, 0.41, and 0.63 series were used and grouped into F values of 10, 11, 12, 13, and 14. This grouping accounts for some of the scatter although some small dependence upon t_w/t_s is evident in the plot of the data.

It is interesting to note that the data consistently correlate with a line whose slope is parallel to the integral multiweb line. Thus, the data indicate that $m = 0.85$ in equation (52) although the value of β_r is not a constant and correlates reasonably well with the F parameter within ±10 percent limits for this series of tests. Furthermore, the lines for the formed channel multiweb beams all lie below that for the integral multiweb beam, even for those subject to local buckling. It is evident, therefore, that all of the beams of this test series experience a reduction in strength from that of the integral multiweb beam which is associated with the low deflectional stiffness of formed channel webs.

W
1
2
2

The results shown in figure 13 can be summarized by using the values of β_r presented in figure 14 in conjunction with the equation

$$\bar{\sigma}_{fr}/\sigma_{cy} = \beta_r\left[\frac{t_s}{b_s}\left(\frac{E}{\sigma_{cy}}\right)^{1/2}\right]^{0.85} \tag{53}$$

The reduction in β_r values for formed channel multiweb beams from $\beta = 1.42$ for integral construction may possibly be associated with an edge strain at the web-cover attachment line which is less than ϵ_{cy} at failure. As a practical design measure, the reduction in strength associated with formed channel webs may be avoided by use of built-up or integral forms of web construction.

Minimum-Weight Design

The preceding portions of this section have been concerned with analyses of buckling and failure of various forms of multiweb beams under bending. At this point, it is pertinent to consider the problem of the design of multiweb beams of minimum weight for specified loading and geometric parameters.

There is a considerable amount of literature devoted to the subject, much of which was reviewed in reference 17. Of necessity, the minimum-weight analyses are concerned with idealized multiweb beams which are representative of integral types of construction employing plate-type covers and webs. The results of analyses pertaining to this type of construction are presented below. The efficiencies of this type of construction as compared with other forms of compression-cover and web construction are presented in a later section.

Optimum number of webs.- Gerard (ref. 39) has considered the optimum design of a multiweb beam with a hinged web-cover attachment. For a wide beam (practically, 3 or more cells) designed so that the web buckles in bending simultaneously with the cover buckling in compression at the design load, the following optimum proportions are obtained:

$$\left(h/b_s\right)_o = 1.12 \tag{54}$$

The optimum number of webs is the integer nearest to

$$n_o = 1.12(w/h) \tag{55}$$

W
1
2
2

In reference 39 an estimate is also given of the weight penalty associated with the use of a number of webs less than the optimum.

Integral-web designs.- Schuette and McCulloch (ref. 29) have presented minimum-weight design charts for wide integral multiweb beams of aluminum and magnesium alloys. More recently, Rosen (ref. 30) has presented charts which include refinements in the strength analysis both for the covers and the webs. In addition, the charts indicate the effects of skin-thickness requirements upon the structural efficiency.

Minimum-weight design charts of reference 30 are shown in figure 15 in terms of specified skin thickness and in terms of cell size. It can be observed in figure 15(b) that the cell proportions for minimum solidity are in good agreement with equation (54).

Corrugated-web designs.- Some increase in the efficiency of multiweb beams can be achieved by the use of corrugated webs in place of the plate type of web associated with figure 15. Fraser (ref. 40) has conducted a limited experimental program on corrugated multiweb beams utilizing one specific form of corrugation configuration with various web-cover attachments.

The results of a minimum-weight analysis based on the experimental results of reference 40 are shown in figure 16. It can be observed that, up to a loading index of approximately 3 ksi (for 7075-T6 aluminum-alloy covers), the corrugated web represents an improvement in efficiency as compared with the plate-type web.

Sandwich multiweb beams.- Increases in the efficiency of multiweb beams may also be achieved by the use of various types of orthotropic-plate compression covers. Of particular interest, currently, is the use of honeycomb-core sandwich plates for the covers of multiweb beams. Although there is relatively little test data on sandwich multiweb beams available, Anderson (ref. 43) has presented some interesting minimum-weight results for this case.

The optimum sandwich-plate configuration is based on the analysis of Semonian and Johnson (ref. 24) which was conducted for a 9.7-lb/cu ft steel honeycomb core bonded to 17-7PH stainless-steel faces. The optimum distribution of supporting structure between the honeycomb core and the corrugated webs was then investigated. The results are presented in figure 17 in terms of specified facing thicknesses. A comparison of the efficiency of this form of construction with that of the other forms considered in this section is presented in the section "Comparative Efficiencies of Thin-Wing Construction."

W
1
2
2

STABILITY OF MULTIPOST BEAMS IN BENDING

The rather large number of webs required for the efficient design of multiweb beams has posed difficult production problems on account of the inaccessibility of the interior webs. As a partial solution to this problem, truss-type construction has been proposed in which the compression cover is stabilized by a series of posts acting in conjunction with the tension cover.

The early stability theories for multipost construction were concerned with the use of a series of posts to support plate-type covers. The results of these theories indicated the necessity of using stiffeners at the line of attachment of the posts to the cover in order to enforce longitudinal nodes in the compression covers of thin wings. Consequently, more recent theories and tests have been devoted to multipost-stiffened beams.

In this section, the available theories for multipost and multipost-stiffened beams are reviewed. Typical results are presented for determining buckling stresses of these types of construction. The few available tests reported in the literature are examined in terms of the theory. It is to be noted that an excellent review of the early development of multipost-stiffened construction has been presented by Badger (ref. 42).

Stability of Spring-Supported Systems

In wing and tail structures, the supporting structure often connects the tension and compression surfaces in a manner analogous to the simplified structural models shown in figure 18. In figure 18(a) the flexural spring (tension member) is effectively rigid and it can be observed that the compression member deflects in its entire length since the deflectional spring is weak. For the strong deflectional spring shown in figure 18(b), a node is enforced at the center which raises the buckling stress of the column above that of the configuration depicted in figure 18(a).

However, if the flexural spring is weak, then a third instability mode is possible in which buckling of the compression and tension bars occurs as a unit as shown in figure 18(c). If the deflectional spring is strong, both bars deflect identically; if weak, the deflection of the compression bar is greater than that of the tension bar.

It is important to note that no increase in buckling stress can be obtained by increasing the spring stiffness beyond the minimum value required to enforce nodes at the spring locations. Thus, from the standpoint of design, considerable interest centers upon the stiffness requirements for the deflectional and flexural springs to act as effectively rigid members.

Seide and Eppler (ref. 43) have considered the buckling of parallel, equally loaded, tension and compression bars connected by one, two, three, and an infinite number of elastic deflectional springs. The analysis indicated that the buckling behavior for more than three springs essentially corresponds to that for an infinite number of springs. Although the analysis of reference 45 pertains to narrow columns, the results can be applied to wide columns by the proper definition of bending rigidities.

For an infinite number of springs connecting a compression cover of rigidity D_c and a tension cover of rigidity D_t, the end-fixity coefficient is given in figure 19. It can be observed that, for the system to be considered effectively rigid, an increase in deflectional-spring stiffness is required to compensate for a decrease in the tension-surface bending rigidity.

The minimum stiffness required of the deflectional spring for the system to be considered effectively rigid was obtained in reference 17. The following relation was derived:

$$KL^3/wD_c = 2\pi^3 s(1 + \cosh \pi s)/\sinh \pi s \tag{56}$$

where

$$s = \left(D_c/D_t\right)^{1/2}$$

For large values of s, equation (56) reduces to

$$KL^3/wD_c = 2\pi^3 s \tag{57}$$

Values of the effectively rigid deflectional-spring stiffness parameter are given as a function of the relative bending rigidities in figure 20.

The line representing equation (56) separates the two regions of possible buckling: The effectively rigid spring and deflected-spring regions. It can be observed that equation (57) is an adequate approximation of equation (56) in the range appropriate to wing and tail designs. Specifically, equation (57) is entirely adequate for values of D_c/D_t greater than 2.

N
1
2
2

Stability of Multipost Beams

The various buckling modes possible with a compression-bar, deflectional-spring, tension-bar system are directly applicable to multipost beams in bending. Specifically, the following modes of instability can occur in multipost construction:

(a) Buckling over several rows of posts due to insufficient rigidity of the posts in a manner analogous to that of figure 18(a)

(b) Transverse nodes, in which chordwise arrays of posts act as effectively rigid members and subdivide the compression cover into a series of short wide columns in a manner analogous to that of figure 18(b)

(c) Displaced posts, in which the entire box becomes unstable as a unit although the posts may be effectively rigid (analogous to figure 18(c))

(d) Longitudinal nodes, in which spanwise arrays of posts act as effectively rigid spars subdividing the compression cover into a series of long narrow plates in the same manner as in a multiweb beam

The stability analysis of multipost beams has been considered in detail by Seide and Barrett (ref. 44). An idealized box beam utilizing post construction and subjected to bending moments, in which the covers are taken as long, simply supported, flat rectangular plates, was analyzed. The covers may be of different flexural rigidities denoted by D_t for the tension cover and D_c for the compression cover. The supporting structure consists of a rectangular array of identical elastic posts which are connected to the covers by pin connections, thereby offering no resistance to rotation of the covers. The transverse and longitudinal post spacings are uniform although generally different.

One of the most significant results of the analysis is presented in figure 21. The regions of the various buckling modes are shown as

functions of the relative bending rigidities of the covers, the ratio of spanwise post spacing to cover width, and the number of chordwise posts n. It can be observed that for a D_t/D_c ratio less than 1, which is the range of interest for wing and tail designs, buckling with longitudinal nodes is impossible. This form of buckling becomes possible only when spanwise stiffeners are used in conjunction with spanwise arrays of posts. Thus, the introduction of multipost-stiffener construction essentially results in another form of multicell construction in which the cover behaves as a long plate. Discussion of this form of construction is presented subsequently.

W
1
2
2

For the range of relative bending rigidities of interest in aircraft design, buckling with transverse nodes or displaced posts are the two possible buckling modes for covers stiffened only by posts. Thus, from the standpoint of design, the minimum axial stiffness of the post system required to enforce transverse nodes is of interest. Such information is contained in reference 44, where the post-stiffness requirements are given as functions of the wide-column aspect ratio L_t/w and bending-rigidity ratio for one, two, or three spanwise rows of posts.

In addition, figure 20 may also be used to evaluate the required post axial stiffness to enforce transverse nodes for L_t/w values less than 0.20. The spring constant of a chordwise row of n elastic posts is

$$K = nA_pE_p/h_p \tag{58}$$

In order to provide some check of the theory of reference 44, Barrett and Seide (ref. 45) have reported the results of a test on a multipost beam in bending containing three spanwise rows of posts between two end shear webs. The axial stiffness of the posts was approximately 5 percent greater than the minimum value required by theory to enforce transverse nodes.

It is significant that the cover buckled with transverse nodes at a stress within 2 percent of that predicted by theory. The structure failed 8 percent beyond the bending moment associated with buckling. The results of the test, however, indicate that significant prebuckling deformations occur in the form of downward dishing of the covers during bending. Such undesirable anticlastic curvature of the beam requires the use of supplemental supporting structures such as ribs or webs.

Stability of Multipost-Stiffened Beams

The inability of an array of posts to enforce longitudinal nodes in the compression cover of a wing and thus serve as a form of construction alternate to a plate-type web has directed attention toward multipost-stiffened construction. Badger (ref. 42) has indicated that the introduction of a longitudinal stiffener at the post-cover attachment line effectively shifts the boundaries delineating the various buckling modes. As shown in figure 22, the use of stiffeners shifts the longitudinal-node boundary into the D_t/D_c range encountered in airframe design.

The theory for multipost-stiffened construction has been developed by Seide (ref. 46). A series of design charts based on this theory is presented in reference 47 for a rather large number of variables. The design charts indicate the value of the stiffener-rigidity parameter γ_c and post-stiffness parameter Υ required to obtain values of $k = 3$, 3.5, and 4.0 for long simply supported plates supported by a multipost-stiffener support at the center. These parameters are defined as follows in reference 47:

$$\gamma_c = EI/b_s D_c \tag{59}$$

$$\Upsilon = Kb_s^3/\pi^4 D_c L_t \tag{60}$$

$$k = \frac{\sigma_{cr} t_c b_s^2}{\pi^2 D_c} \tag{61}$$

Other variables included in these design charts are ratios of post spacing to plate width $L_t/b_s = 0$, 1/2, 1, and 2 and cover-stiffness ratios $D_t/D_c = 1/8$, 1, and ∞.

In figure 23, results were taken from reference 47 for $L_t/b_s = 1$ and 2 for a k value of 4 which indicate that the post-stiffener combination enforces a node in the cover. The results for $D_t/D_c = 1/8$ and 1 which cover the range of interest in airframe design closely coincide in figure 23. Thus it appears reasonable to use these results for intermediate values of D_t/D_c.

Effectively rigid system.- The minimum conditions under which an effectively rigid system is obtained are of interest for multipost-stiffened construction as well as for multipost construction. Figure 23 presents this information in terms of the required values of Υ for a range of γ_c values. It is important to note that, at the right side of figure 23, minimum values of γ_c are reached. Since the minimum stiffener size is required in this region, it is of particular interest to know the minimum value of Υ associated with each minimum value of γ_c.

Although this information is displayed in figure 23, it is convenient to have available an approximate method of analysis for establishing the minimum post conditions for the effectively rigid system of smallest stiffener rigidity. This is particularly true since figure 23 shows a large number of parameters and interpolation procedures are not readily evident.

The minimum rigidity required for a central longitudinal stiffener to enforce longitudinal nodes in simply supported plates of various lengths was obtained in reference 17. The values of γ_c needed to obtain $k = 4$ in equation (61) are presented in the following table where $\bar{t} = t_c + \left(nA_s/w\right)$.

L_t/b_s	$\bar{t}/t_c = 1.0$ γ_c	$\bar{t}/t_c = 1.2$ γ_c	$\bar{t}/t_c = 1.4$ γ_c
1	4.4	5.2	6.0
2	14.4	17.6	20.8
3	27.4	34.6	41.8

In a multipost-stiffened beam, the posts are used to enforce nodes in the stiffener at the post locations and thereby reduce the effective stiffener length. Thus, the post-stiffener combination tends to act in a manner analogous to that shown in figure 18. By employing the procedure of reference 17, the post-stiffener requirements may be determined.

By neglecting the compression and tension skins, the minimum post axial stiffness to enforce nodes in the stiffener can be obtained directly from figure 20 by multiplying D by γ_c. Thus, by use of equations (57) and (60),

$$\Upsilon = (2/\pi)\gamma_c\left(b_s/L_t\right)^4 \tag{62}$$

where the γ_c values associated with a particular L_t/b_s may be determined from the foregoing table.

The results of this approximate analysis are shown in figure 23 for comparison with the theory of reference 47. It can be observed that the approximate results are conservative and in relatively good agreement with the more exact analysis. For design purposes, the minimum γ_c and Υ values are summarized in figure 24.

W
1
2
2

Beam tests.- A limited number of tests on multipost-stiffened beams under bending have been reported in the literature (refs. 36 and 42). These tests were designed to obtain information on the behavior of this form of construction rather than to provide a basic check of the theory.

Badger (ref. 42) has summarized the results of three bending tests on large-scale multipost-stiffened beams which closely simulated actual wing design. The results indicated that the behavior was similar to multiweb construction in that the theoretical buckling stresses were experimentally confirmed for extruded stiffeners whereas premature failure was experienced when formed stiffeners were used in the tests. In addition to the bending tests, results on a multipost-stiffened beam under torsion were also reported.

Johnson (ref. 36) has conducted a series of tests on various types of multipost-stiffened beams under bending. The beams consisted of 2014-T6 rectangular cross-section tubing stiffened along the center line by various 7075-T6 aluminum-alloy post-stiffener combinations of approximately the same weight so as to form square cells. Also tested for reference purposes was a built-up 7075-T6 aluminum-alloy web such as that used in multiweb construction.

The multipost-stiffener structures utilized extruded Z-stiffeners supported by angle sections at spacings of $L_t/b_s = 1/2$, 1, and 2. In a fourth multipost-stiffener beam, the posts were inclined to form a Warren truss which is capable of carrying shear loads. In terms of the parameters of figure 23, $D_t/D_c = 1$, the stiffeners had values of $\gamma_c = 1{,}600$ and $\bar{t}/t_c = 1.5$, and for the posts $\Upsilon = 1.87$, 3.44, and 4.52 for $L_t/b_s = 2$, 1, and 1/2, respectively. For the Warren truss arrangement, $\Upsilon = 1.41$ for $L_t/b_s = 15/8$.

The results of these tests are summarized in figure 25 where the bending moments for buckling and failure of the multipost-stiffened beams are compared with those for a multiweb beam. It can be observed that the buckling moment increases as the post spacing decreases and that the values are below that for the multiweb beam. In all cases, the predicted M_{cr} was approximately equal to that of the multiweb. In

reference 36, the low value of the experimental M_{cr} as compared with the theoretical was attributed to initial waviness of the rectangular tube.

The corresponding M_f values are closer to that for the multiweb beam. At $L_t/b_s = 1/2$, the multipost-stiffened beam achieved a failing strength comparable with that of the multiweb beam. It is interesting to note that the test points for the Warren truss arrangement are somewhat higher than those for a multipost-stiffened beam of comparable L_t/b_s. It is apparent from this series of tests that strength levels comparable with those of integral multiweb beams can be achieved by multipost-stiffener arrangements of relatively high deflectional stiffness.

W
1
2
2

Minimum-Weight Designs

Gerard (ref. 17) has considered the minimum-weight design of multipost beams and has concluded that the optimum post weight should approach 1/3 of the cover weight. Information on the optimum post spacing is presented. Certain minimum-weight aspects of multipost-stiffener construction are also considered in reference 17.

COMPARATIVE EFFICIENCIES OF THIN-WING CONSTRUCTION

In the preceding portions of this report, various forms of thin-wing construction have been discussed. The design aspects as distinct from the strength analysis are contained in the minimum-weight design sections for each of the forms of construction considered herein. A further design consideration of importance is concerned with the comparative efficiencies of the various forms of construction. This final section is devoted, therefore, to a summary of comparative efficiency studies of compression covers, web systems, and multicellular thin-wing box beams.

In order to compare the weight efficiencies of various competing forms of construction, it is necessary to introduce various idealizations into the analysis to reduce the wide range of variables to a common set of parameters. The results obtained from such analyses can thus serve as a guide to the designer in selecting the minimum-weight structural configuration based on certain prescribed loading and geometric parameters as shown in reference 17.

In passing, it is worth noting that such analyses can also be used to determine the weight efficiency of various materials, particularly

at elevated temperatures. Analyses of this type are presented in some detail in reference 48.

Compression Covers

A common form of multicell construction utilizes a relatively thick tapered plate supported by a series of longitudinal webs. The efficiency of a multicellular arrangement in thin wings has encouraged investigations concerned with the rearrangement and reduction of structural material within the cover plate with the objective of obtaining decreased solidity and, therefore, increased weight efficiency. As a consequence, the following forms of orthotropic-plate construction have been studied: Longitudinally stiffened plates, transversely stiffened plates, and waffle-grid plates as well as corrugated-core and honeycomb types of sandwich plates.

Because of the relatively large variety of plate types of construction, the minimum-weight or optimum configurations of each type of orthotropic-plate construction were investigated in reference 2. The comparative efficiencies of the various types of plates under compressive loading were then examined with the results shown in figure 26. The conclusions presented in reference 2 and shown in figure 26 are as follows:

(a) Longitudinally and transversely stiffened plates are comparable in efficiency to unstiffened plates in compression and consequently do not represent any significant improvement over unstiffened plates.

(b) Sandwich plates with unidirectionally weak corrugated cores oriented longitudinally are comparable in efficiency to waffle-grid construction. Both types represent a significant increase in efficiency over the unstiffened plate.

(c) Sandwich plates with honeycomb or strong corrugated cores represent really significant increases in efficiencies as compared with unstiffened plates. For elastic buckling, however, the honeycomb-core sandwich appears to be more efficient than a sandwich plate utilizing a corrugated type of core which is strong in shear.

The foregoing conclusions are based on the behavior of the various forms of stiffened plates in the region where stability rather than strength governs. It is apparent from figure 26 that the honeycomb sandwich plate is of superior efficiency by virtue of reaching the 45°-strength-limit lines at the lowest value of the structural loading parameter $N/\bar{E}w$. However, once strength limitations govern, the present type of analysis is no longer valid and it is necessary to conduct analyses such as those given in references 2 and 24.

Web Systems

Web systems employed in multiweb wings perform a dual function. Under pure bending, the webs in conjunction with the tension cover act as the supporting structure for the compression cover. In addition, the webs carry the shear loads acting on any wing structure.

The supporting structural requirements for the web system under pure bending have been discussed in the sections devoted to multiweb and multipost beams. Certain of the minimum-weight aspects of the supporting structure have also been considered in reference 17.

W
1
2
2

Although the supporting function of the web system places a lower limit on the geometry of the web structure, it is often found in wing design that the shear-load requirements dictate the details of the web system. Consequently, this section is devoted to a summary of the minimum-weight aspects of shear webs. This summary is based on rather scattered data and should be used only as a rather general guide in design.

Tension-field webs.- Kuhn (ref. 49) has presented the results of a series of calculations leading to minimum-weight designs of 2024-T3 and 7075-T6 aluminum-alloy tension-field webs. Because of an apparent similarity between the shear strength of stiffened webs and the crippling strength of stiffened panels, Kuhn's minimum-weight results were correlated in terms of parameters similar to those used in the crippling analysis of reference 1.

The results of this correlation are shown in figure 27 where the shear constants τ_y and G have been used in place of σ_{cy} and E. It can be observed that the minimum-weight designs for the two aluminum alloys essentially form a single curve in terms of the parameters of figure 27. This suggests that figure 27 may be useful in establishing minimum-weight designs for values of τ_y other than those used by Kuhn in establishing the basic results.

Shear-resistant webs.- Symonds (ref. 50) has considered the minimum-weight design of shear-resistant web systems of 2024-T3 aluminum alloy. The results of his calculations are presented in figure 28 together with those for tension-field webs as well as several other types. Symonds found that the efficiency increased as the stiffener spacing decreased. For a stiffener spacing of $b_s = 0.2b_w$, the efficiency of the shear-resistant web is greater than that of the tension-field web beyond a loading index of 100 psi (for 2024-T3).

Shanley (ref. 51) has presented a considerable amount of test data on the strength of 2024-T3 aluminum-alloy webs containing beaded lightening holes. An envelope of the upper limits of the test data taken from reference 51 is shown in figure 28.

Also shown are some test data on the shear strength of 2024-T3 aluminum-alloy flat corrugated webs as taken from reference 53. Basically, the corrugated web represents a shear-resistant web of very close stiffener spacing with a consequent high efficiency.

Unstiffened webs.- For reference purposes, the buckling strength of a long unstiffened web in shear is also shown in figure 28. These results were calculated from

$$\tau_o = \left[\frac{\pi^2 k_s}{12\left(1 - \nu_e^2\right)}\right]^{1/3} (\eta E)^{1/3}\left(q/b_w\right)^{2/3} \tag{63}$$

Also shown are the results of some calculations for a long honeycomb-sandwich web in shear with a face-core density of 50. The analysis is similar to that presented in reference 2 for compressed sandwich plates with a facing stress equal to the shear yield strength. It can be observed that sandwich construction is highly efficient for web systems, particularly at low values of the loading index. This result coincides with that obtained for compressed orthotropic plates.

Generalizations for web systems.- For the various minimum-weight shear web systems considered above, buckling has been assumed to occur in only one mode. Consequently, the optimum shear stress in terms of the loading index for shear-resistant web systems is

$$\bar{\tau}_o = \alpha_s (\eta E)^{1/3}\left(q/b_w\right)^{2/3} \tag{64}$$

where

$$\alpha_s = \left[\frac{\pi^2 k_s}{12\left(1 - \nu_e^2\right)}\right]^{1/3} \bar{t}/t$$

$$\eta = \left(\frac{1 - \nu_e^2}{1 - \nu^2}\right) G_s/G$$

All of the data shown in figure 28 with the exclusion of tension-field webs correlate with lines of slope equal to 2/3 in the elastic region in accordance with equation (64). The values of α_s in the elastic range can be determined directly from figure 28 and are presented in the following table.

Type of system	α_s	Remarks
Unstiffened	1.7	Theory
Shear resistant	3.7	$b_s/b_w = 0.2$
Lightening holes	4.0	Test data
Flat corrugation	12	Test data
Honeycomb sandwich	17	$\varphi/\bar{\varphi} = 50$

W
1
2
2

These results permit possible extension of the data presented in figure 28 for 2024-T3 aluminum alloy to other materials. In conjunction with the data of figure 27 for minimum-weight tension-field web systems, a generalized approach to the minimum-weight design of web systems may be possible. However, since these results are based on data from scattered sources, any generalized approach must be viewed with some caution. A completely analytical approach to a minimum-weight shear web such as presented in reference 2 for orthotropic plates in compression would appear to be highly desirable.

Multicellular Beams

The various types of compression covers in conjunction with the various web-system supporting structures form a large variety of multicellular beams for use in thin-wing construction. The comparative efficiencies of only a few of the possible beam configurations have been investigated. It is important to note, however, that the methods of analysis are sufficiently general so as to be applicable to a wide variety of combinations of cover and web configurations in multicellular beams.

An early attempt to establish the conditions where integral plate-type multiweb construction may be efficiently employed was presented in reference 17. This analysis indicated that efficient application of plate-type multiweb construction as compared with stiffened-panel construction, for example, required an optimum stress level in the compression cover in the region of the compressive yield strength. It was also

concluded that a multipost beam of optimum design may be somewhat more efficient than a multiweb beam in the loading-index range corresponding to the elastic range.

In order to extend the loading-index range in which multiweb construction may be efficiently employed, the use of sandwich plate covers has been considered. Anderson (ref. 41) has evaluated the comparative efficiencies of integral multiweb beams with plate-type and corrugated webs, and honeycomb-sandwich—corrugated-web beams. The results of this analysis are shown in figure 29. It is important to note that although the sandwich beam is of stainless steel, it has greater efficiency in the loading-index range below 2 ksi than do the aluminum-alloy-plate types of construction.

Research Division, College of Engineering,
New York University,
New York, N. Y., December 23, 1957.

APPENDIX A

APPLICATION SECTION

In this application section, the results contained in this part of the Handbook are summarized for convenient use in the design and analysis of thin-wing forms of construction.

Orthotropic Flat Plates

W
1
2
2

General charts for the compressive and shear buckling of orthotropic flat plates with various boundary conditions are presented in figures 3 and 4. For plates in which shear deformability may be of importance, such as sandwich plates, buckling charts for compression and shear are presented in figure 6.

The use of figures 3, 4, and 6 requires a knowledge of the elastic constants of the plate. Available theoretical and experimental procedures for evaluating the pertinent constants are reviewed in the section "Stability of Orthotropic Flat Plates."

Multiweb Beams

Buckling stresses.- The local buckling strength of multiweb beams may be determined from

$$\sigma_{cr} = \frac{\pi^2 k \eta E}{12\left(1 - \nu_e^2\right)}\left(\frac{t_s}{b_s}\right)^2 \tag{33}$$

For integral beams, k may be determined from figure 8. For built-up webs, significant rotational restraint may occur at the cover-web attachment. In such cases, k may be evaluated according to methods presented in references 29 and 32.

Beams employing formed channel webs may be subject to wrinkling instability associated with the low deflectional stiffness of the webs in addition to local buckling. In such cases, equation (33) may be used in conjunction with k values from figure 9. The plasticity-reduction factors for use in equation (33) are given by equations (35), (36), (38), and (46) in the section "Buckling and Failure of Multiweb Beams in Bending."

In addition to local buckling and wrinkling, the webs may be subject to crushing instability. As a practical measure, web crushing generally does not occur in stiffened webs. In cases where crushing may be of importance, equations (43) and (48) may be utilized.

Failure strength.- The crippling strength of the compression cover of multiweb beams in bending subject to local or wrinkling instability may be determined from

W
1
2
2

$$\bar{\sigma}_f/\sigma_{cy} = \beta\left[\frac{t_s}{b_s}\left(\frac{E}{\sigma_{cy}}\right)^{1/2}\right]^{0.85} \tag{53}$$

The crippling coefficient β depends upon the rotational and deflectional stiffness of the webs in each form of construction as follows:

Multiweb type		β
Integral		1.42
Built-up	k	β
	4	1.42
	5.35	1.60
	6.35	1.75
Formed channel	F	[a] β_r
	10	1.32
	11	1.19
	12	1.07
	13	.99
	14	.87

[a]For $p/d = 3$, $r_w/t_w = 4$.

Multipost Beams

From a design standpoint, the post axial stiffness required for the posts to act as effectively rigid members is of considerable interest. This information is contained in reference 44 and may be determined approximately from figure 20.

For multipost-stiffener beams, the requirements for an effectively rigid supporting system which enforces longitudinal nodes in the cover are presented in figure 23. Approximate (conservative) requirements for the posts and stiffener are also presented in figure 24.

REFERENCES

1. Gerard, George: Handbook of Structural Stability. Part V - Compressive Strength of Flat Stiffened Panels. NACA TN 3785, 1957.

2. Gerard, George: Minimum Weight Analysis and Comparative Efficiencies of Orthotropic Plates Under Compressive Loading. Tech. Rep. SM 57-6, Contract NAw-6482, NACA and New York Univ., Sept. 1957.

3. Becker, Herbert: Handbook of Structural Stability. Part II - Buckling of Composite Elements. NACA TN 3782, 1957.

4. Timoshenko, Stephen: Theory of Plates and Shells. McGraw-Hill Book Co., Inc., 1940, pp. 188-190.

5. Libove, Charles, and Batdorf, S. B.: A General Small-Deflection Theory for Flat Sandwich Plates. NACA Rep. 899, 1948. (Supersedes NACA TN 1526.)

6. Libove, Charles, and Hubka, Ralph E.: Elastic Constants for Corrugated-Core Sandwich Plates. NACA TN 2289, 1951.

7. Wittrick, W. H.: Correlation Between Some Stability Problems for Orthotropic and Isotropic Plates under Bi-Axial and Uni-Axial Direct Stress. Aero. Quart., vol. 4, pt. 1, Aug. 1952, pp. 83-92.

8. Hayashi, T.: Torsional Buckling of Orthogonal Anisotropic Cylinders. Presented at Eighth Int. Cong. Theor. and Appl. Mech. (Istanbul, Turkey), Aug. 1952. (Reprint.)

9. Seydel, Edgar: The Critical Shear Load of Rectangular Plates. NACA TM 705, 1933.

10. Gerard, George, and Becker, Herbert: Handbook of Structural Stability. Part I - Buckling of Flat Plates. NACA TN 3781, 1957.

11. Sandorff, P. E.: Design of Structural Models with Application to Stiffened Panels Under Combined Shear and Compression. Jour. Aero. Sci., vol. 23, no. 7, July 1956, pp. 623-632.

12. Seide, Paul, and Stowell, Elbridge Z.: Elastic and Plastic Buckling of Simply Supported Solid-Core Sandwich Plates in Compression. NACA Rep. 967, 1950. (Supersedes NACA TN 1822.)

13. Seide, Paul: Compressive Buckling of Flat Rectangular Metalite Type Sandwich Plates With Simply Supported Loaded Edges and Clamped Unloaded Edges (Revised). NACA TN 2637, 1952. (Supersedes NACA TN 1886.)

14. Seide, Paul: Shear Buckling of Infinitely Long Simply Supported Metalite Type Sandwich Plates. NACA TN 1910, 1949.

15. Seide, Paul, and Stein, Manuel: Compressive Buckling of Simply Supported Plates with Longitudinal Stiffeners. NACA TN 1825, 1949.

16. Seide, Paul: The Effect of Longitudinal Stiffeners Located on One Side of a Plate on the Compressive Buckling Stress of the Plate-Stiffener Combination. NACA TN 2873, 1953.

17. Gerard, George: Minimum-Weight Analysis of Compression Structures. New York Univ. Press (New York), 1956.

18. Gomza, Alexander, and Seide, Paul: Minimum-Weight Design of Simply Supported Transversely Stiffened Plates Under Compression. NACA TN 1710, 1948.

19. Dow, Norris F., Levin, L. Ross, and Troutman, John L.: Elastic Buckling Under Combined Stresses of Flat Plates with Integral Waffle-Like Stiffening. NACA TN 3059, 1954.

20. Dow, Norris F., Libove, Charles, and Hubka, Ralph E.: Formulas for Elastic Constants of Plates with Integral Waffle-Like Stiffening. NACA Rep. 1195, 1954. (Supersedes NACA RM L53E13a.)

21. Crawford, Robert F., and Libove, Charles: Shearing Effectiveness of Integral Stiffening. NACA TN 3443, 1955.

22. Crawford, Robert F.: A Theory for the Elastic Deflections of Plates Integrally Stiffened on One Side. NACA TN 3646, 1956.

23. Anon.: Sandwich Construction for Aircraft. Part II - Materials Properties and Design Criteria. ANC-23, Munitions Board Aircraft Committee, May 1951.

24. Johnson, Aldie E., Jr., and Semonian, Joseph W.: A Study of the Efficiency of High-Strength, Steel, Cellular-Core Sandwich Plates in Compression. NACA TN 3751, 1956.

25. Bijlaard, P. P.: Optimum Distribution of Material in Sandwich Plates Loaded in Their Plane. Rep. SA-247-S-8, Cornell Aero. Lab., Inc., Mar. 15, 1950.

26. Anderson, Melvin S., and Updegraff, Richard G.: Some Research Results on Sandwich Structures. NACA TN 4009, 1957.

27. Seide, Paul: The Stability Under Longitudinal Compression of Flat Symmetric Corrugated-Core Sandwich Plates with Simply Supported Loaded Edges and Simply Supported or Clamped Unloaded Edges. NACA TN 2679, 1952.

28. Anderson, Roger A., and Semonian, Joseph W.: Charts Relating the Compressive Buckling Stress of Longitudinally Supported Plates to the Effective Deflectional and Rotational Stiffness of the Supports. NACA Rep. 1202, 1954. (Supersedes NACA TN 2987.)

29. Schuette, Evan H., and McCulloch, James C.: Charts for the Minimum-Weight Design of Multiweb Wings in Bending. NACA TN 1323, 1947.

30. Rosen, B. Walter: Analysis of the Ultimate Strength and Optimum Proportions of Multiweb Wing Structures. NACA TN 3633, 1956.

31. Eggwertz, Sigge F.: Buckling Stresses of Box-Beams Under Pure Bending. Rep. No. 33, The Aero. Res. Inst. of Sweden (Stockholm), 1950.

32. Bijlaard, P. P., and Johnston, G. S.: Compressive Buckling of Plates Due to Forced Crippling of Stiffeners. Preprint No. 408, S.M.F. Fund Paper, Inst. Aero. Sci., Jan. 1953.

33. Semonian, Joseph W., and Anderson, Roger A.: An Analysis of the Stability and Ultimate Bending Strength of Multiweb Beams with Formed-Channel Webs. NACA TN 3232, 1954.

34. Pride, Richard A., and Anderson, Melvin S.: Experimental Investigation of the Pure-Bending Strength of 75S-T6 Aluminum-Alloy Multiweb Beams with Formed-Channel Webs. NACA TN 3082, 1954.

35. Eggwertz, Sigge F.: Strength of 75S-T Integral Compression Skins in Box-Beams Under Pure Bending. Rep. No. 64, The Aero. Res. Inst. of Sweden (Stockholm), 1956.

36. Johnson, Aldie E., Jr.: Bending Tests on Box Beams Having Solid- and Open-Construction Webs. NACA TN 3231, 1954.

37. Gerard, George: Handbook of Structural Stability. Part IV - Failure of Plates and Composite Elements. NACA TN 3784, 1957.

38. Needham, Robert A.: The Ultimate Strength of Multiweb Box Beams in Pure Bending. Jour. Aero. Sci., vol. 22, no. 11, Nov. 1955, pp. 781-876. (See also Comments by Richard A. Pride, Jour. Aero. Sci., vol. 23, no. 11, Nov. 1956. pp. 1059-1060.)

39. Gerard, George: Optimum Number of Webs Required for a Multicell Box Under Bending. Jour. Aero. Sci., vol. 15, no. 1, Jan. 1948, pp. 53-56.

40. Fraser, Allister F.: Experimental Investigation of the Strength of Multiweb Beams with Corrugated Webs. NACA TN 3801, 1956.

41. Anderson, R. A.: Weight-Efficiency Analysis of Thin-Wing Construction. Trans. ASME, vol. 79, no. 5, July 1957, pp. 974-979.

42. Badger, D. M.: Analysis and Design of Multipost-Stiffened Wings. Aero. Eng. Rev., vol. 12, July 1953, pp. 45-57.

43. Seide, Paul, and Eppler, John F.: The Buckling of Parallel Simply Supported Tension and Compression Members Connected by Elastic Deflectional Springs. NACA TN 1823, 1949.

44. Seide, Paul, and Barrett, Paul F.: The Stability of the Compression Cover of Box Beams Stiffened by Posts. NACA Rep. 1047, 1951. (Supersedes NACA TN 2153.)

45. Barrett, Paul F., and Seide, Paul: An Experimental Determination of the Critical Bending Moment of a Box Beam Stiffened by Posts. NACA TN 2414, 1951.

46. Seide, Paul: Derivation of Stability Criterions for Box Beams with Longitudinally Stiffened Covers Connected by Posts. NACA TN 2760, 1952.

47. Anderson, Roger A., Johnson, Aldie E., Jr., and Wilder, Thomas W., III: Design Data for Multipost-Stiffened Wings in Bending. NACA TN 3118, 1954.

48. Gerard, George: Thermostructural Efficiencies of Compression Elements and Materials. Trans. ASME, vol. 79, no. 5, July 1957, pp. 967-973.

49. Kuhn, Paul: Stresses in Aircraft and Shell Structures. McGraw-Hill Book Co., Inc., 1956, pp. 66-75.

50. Symonds, Malcolm F.: Minimum Weight Design of a Simply Supported Transversely Stiffened Plate Loaded in Shear. Jour. Aero. Sci., vol. 23, no. 7, July 1956, pp. 685-693.

51. Shanley, Francis Reynolds: Weight-Strength Analysis of Aircraft Structures. McGraw-Hill Book Co., Inc., 1952, pp. 38-40.

W
1
2
2

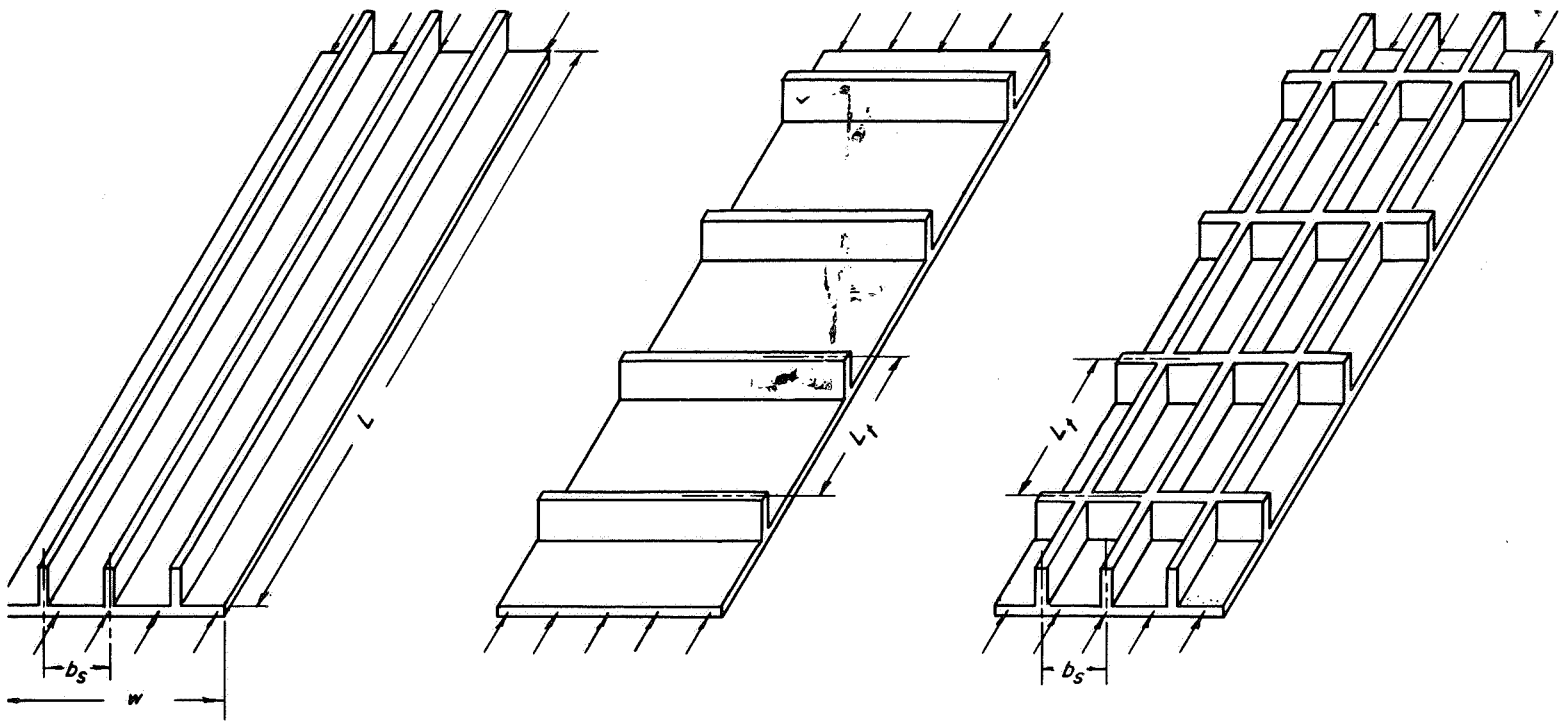

(a) Longitudinal stiffening. (b) Transverse stiffening. (c) Waffle-grid stiffening.

Figure 1.- Classification of stiffening systems for single- and double-skin construction.

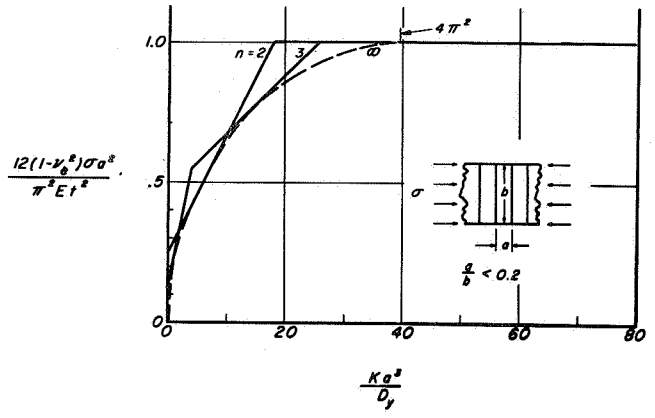

(a) Transversely stiffened plate in compression.

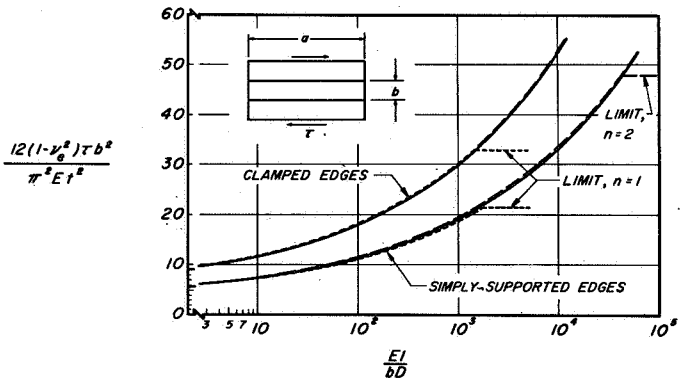

(b) Longitudinally stiffened plate in shear.

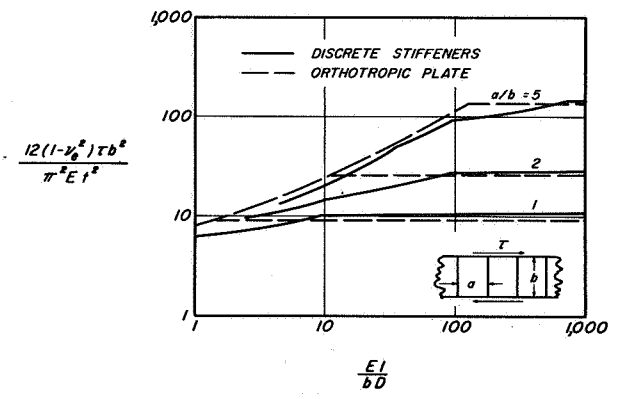

(c) Transversely stiffened plate in shear.

Figure 2.- Comparison of orthotropic buckling stresses for stiffened plates with stresses found from multiple-stiffener theory.

W-122

W-122

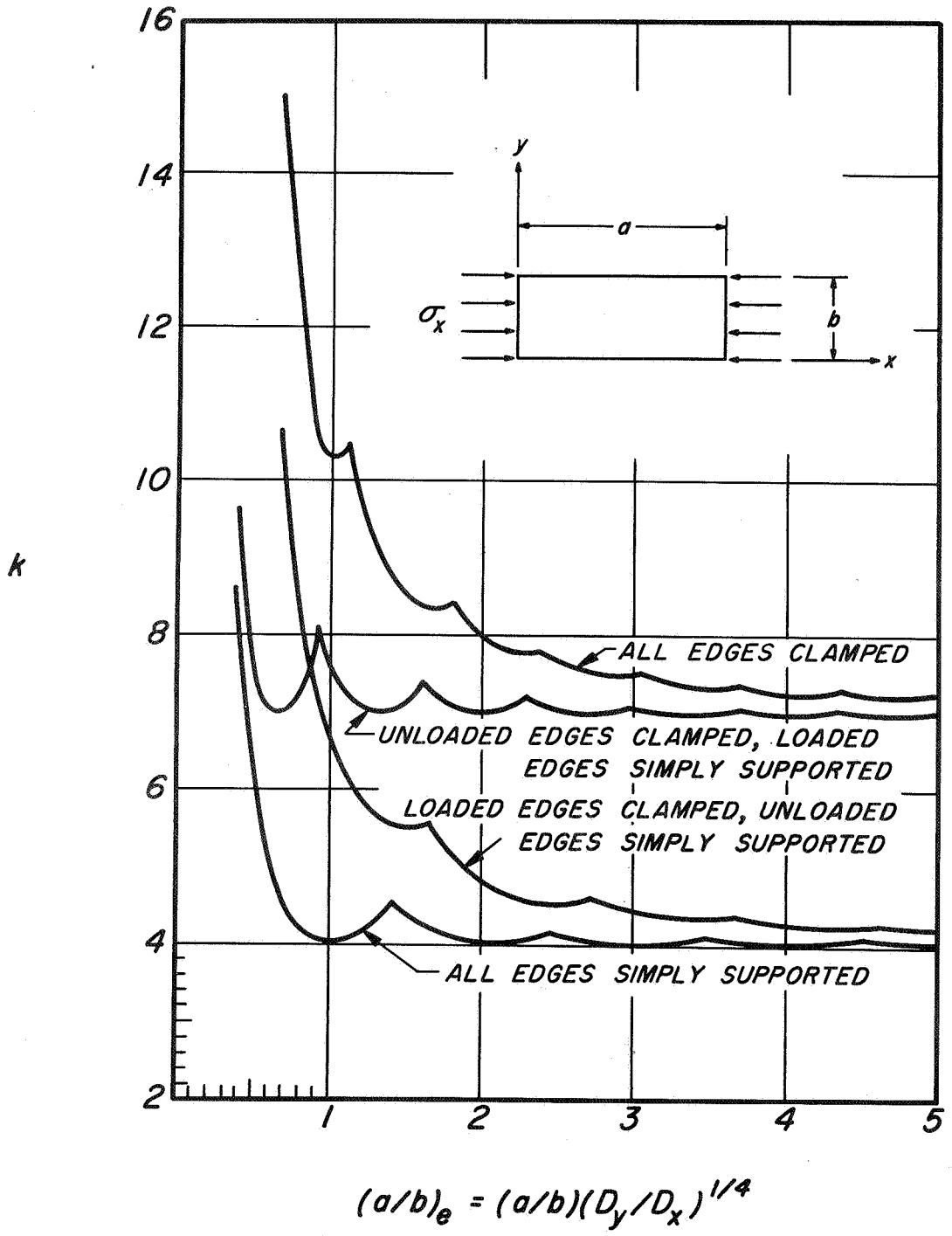

Figure 3.- Compressive buckling coefficients for flat rectangular orthotropic plates.

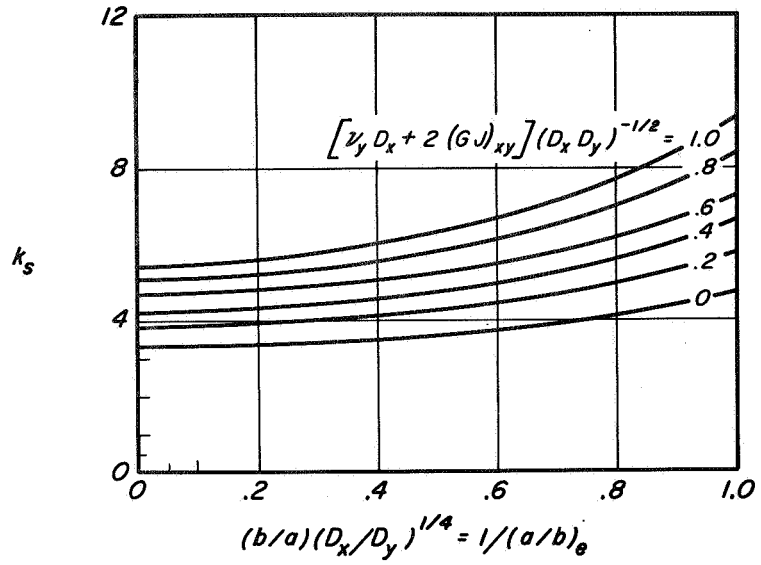

(a) All edges simply supported.

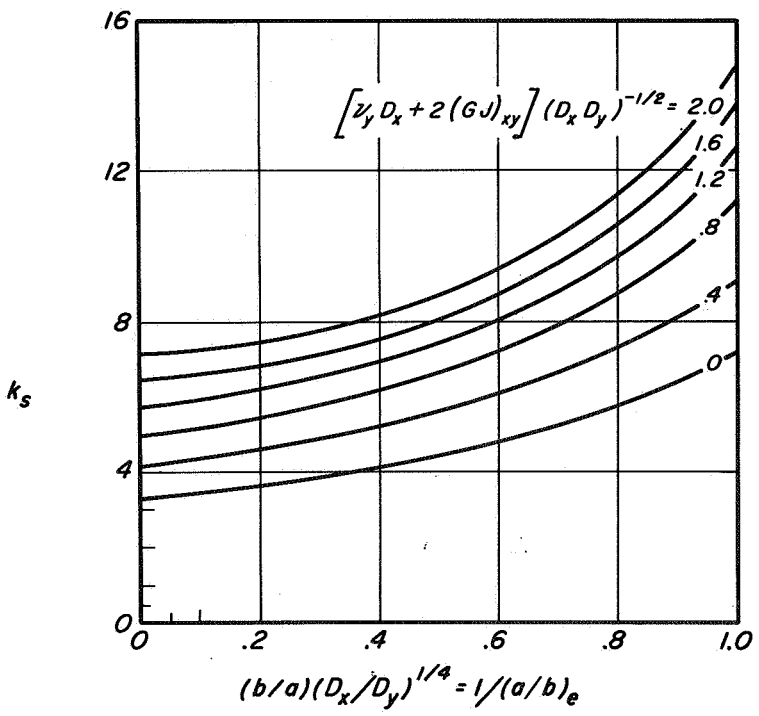

(b) Short edges clamped, long edges simply supported.

Figure 4.- Shear-buckling coefficients for orthotropic plates (data taken from refs. 4 and 19).

W-122

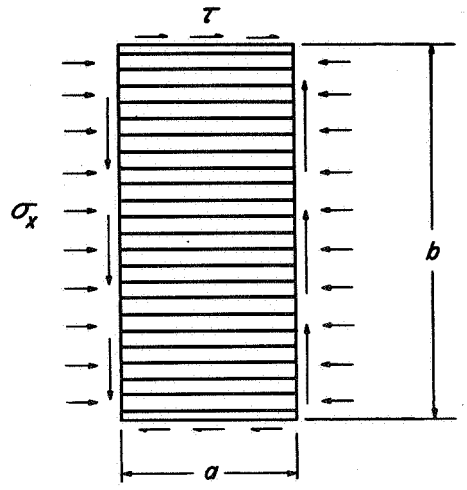

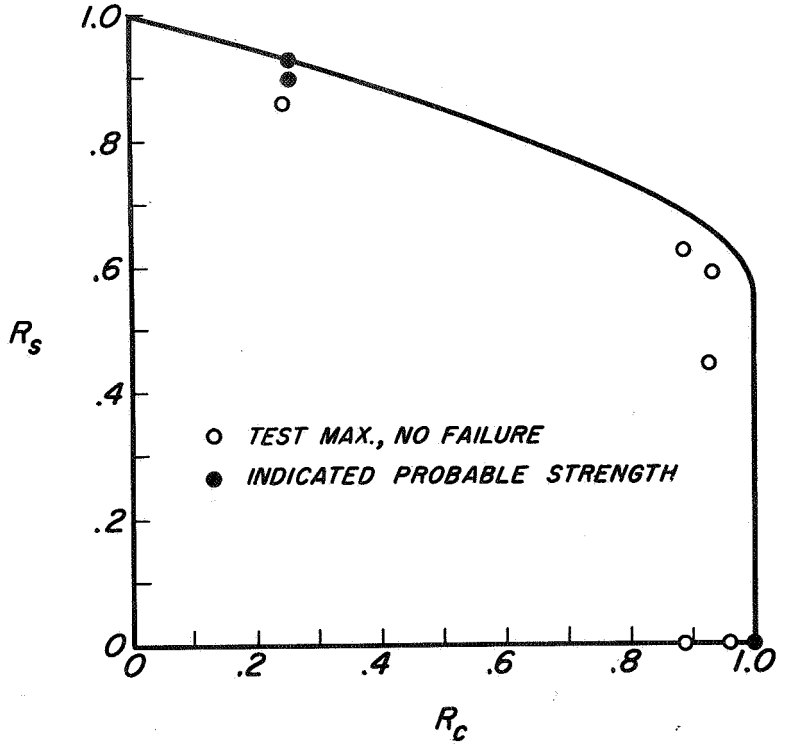

Figure 5.- Interaction data for stiffened wide column under combined compression and shear taken from reference 11.

W-122

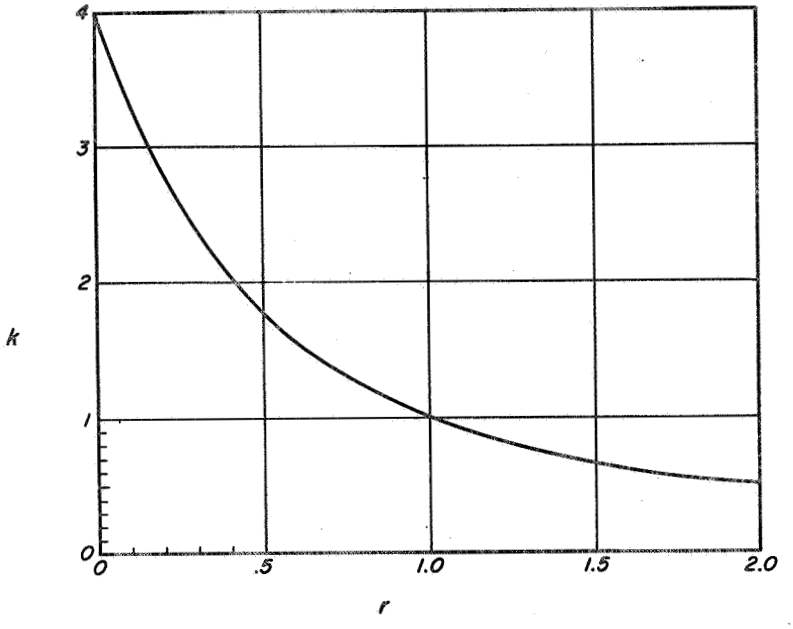

(a) Long simply supported sandwich plates in longitudinal compression.

For $r \leqq 1$, $k = \frac{4}{(1 + r)^2}$; $r \geqq 1$, $k = \frac{1}{r}$.

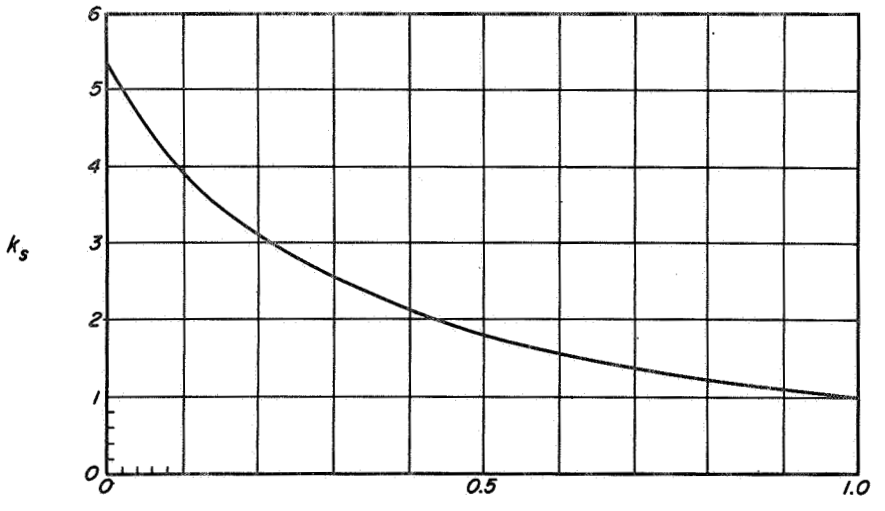

(b) Long simply supported sandwich plates in shear.

Figure 6.- Instability coefficients for long sandwich plates (refs. 12 and 14).

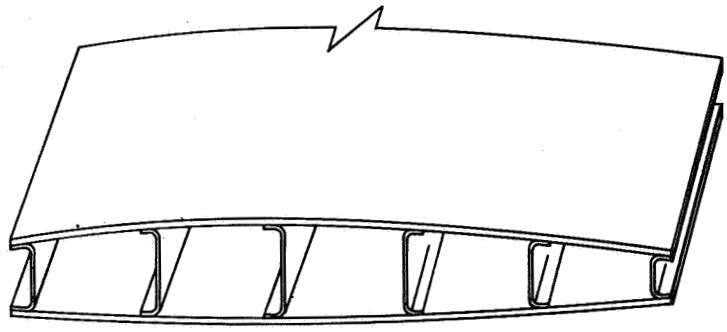

MULTIWEB WING SECTION

W-122

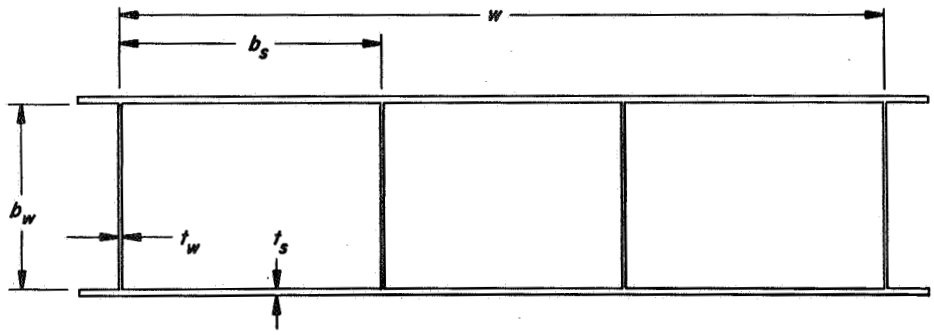

INTEGRAL WEBS

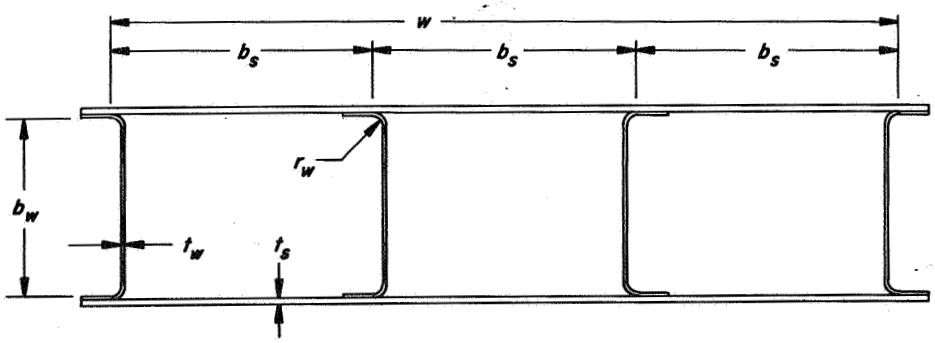

FORMED CHANNEL WEBS

Figure 7.- Forms of multiweb construction.

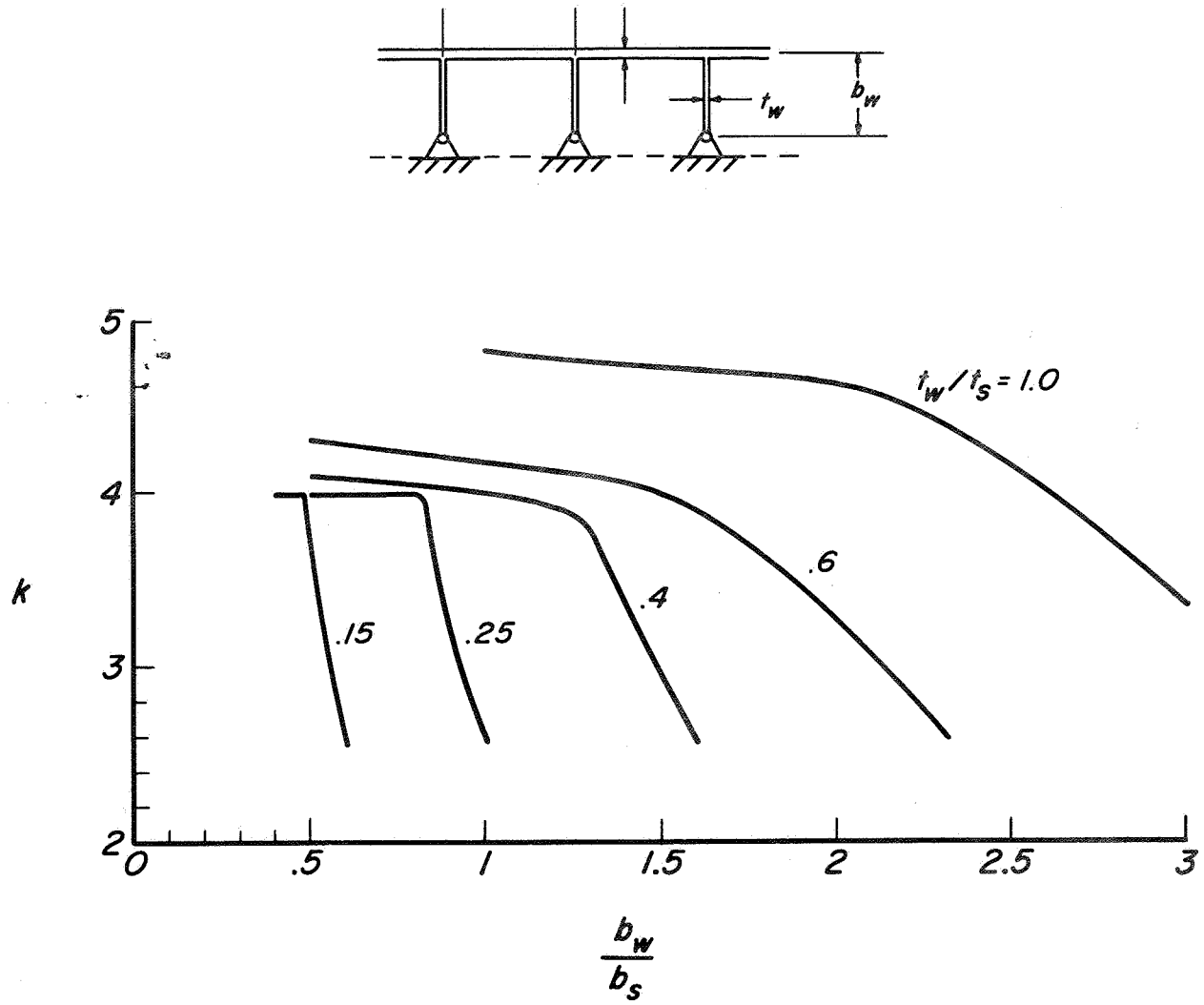

Figure 8.- Instability coefficients for wide, idealized, integral, multiweb box beams under bending (ref. 29).

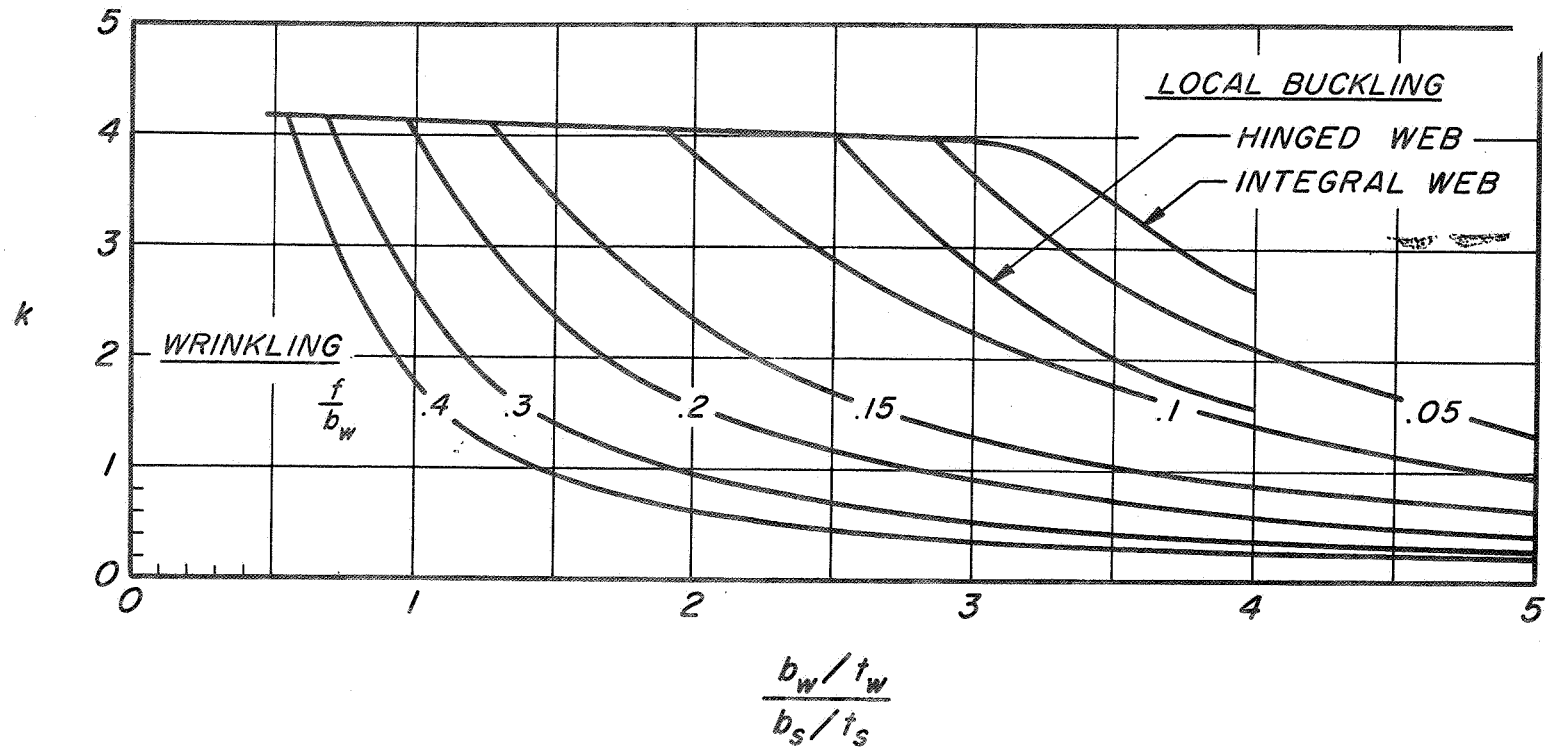

Figure 9.- Wrinkling instability and local buckling of multiweb box beams under bending (ref. 33).

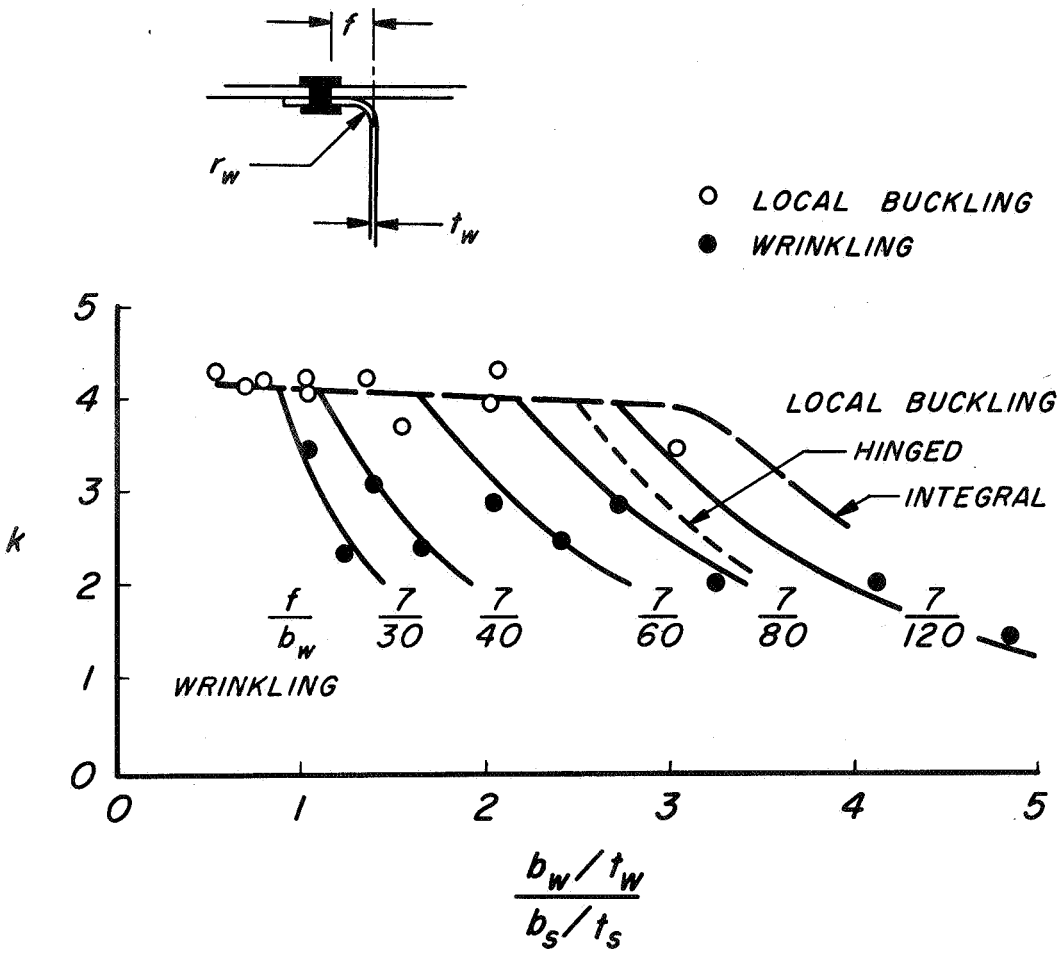

Figure 10.- Comparison of test data and theory for buckling of formed channel multiweb box beams under bending (ref. 33).

W-122

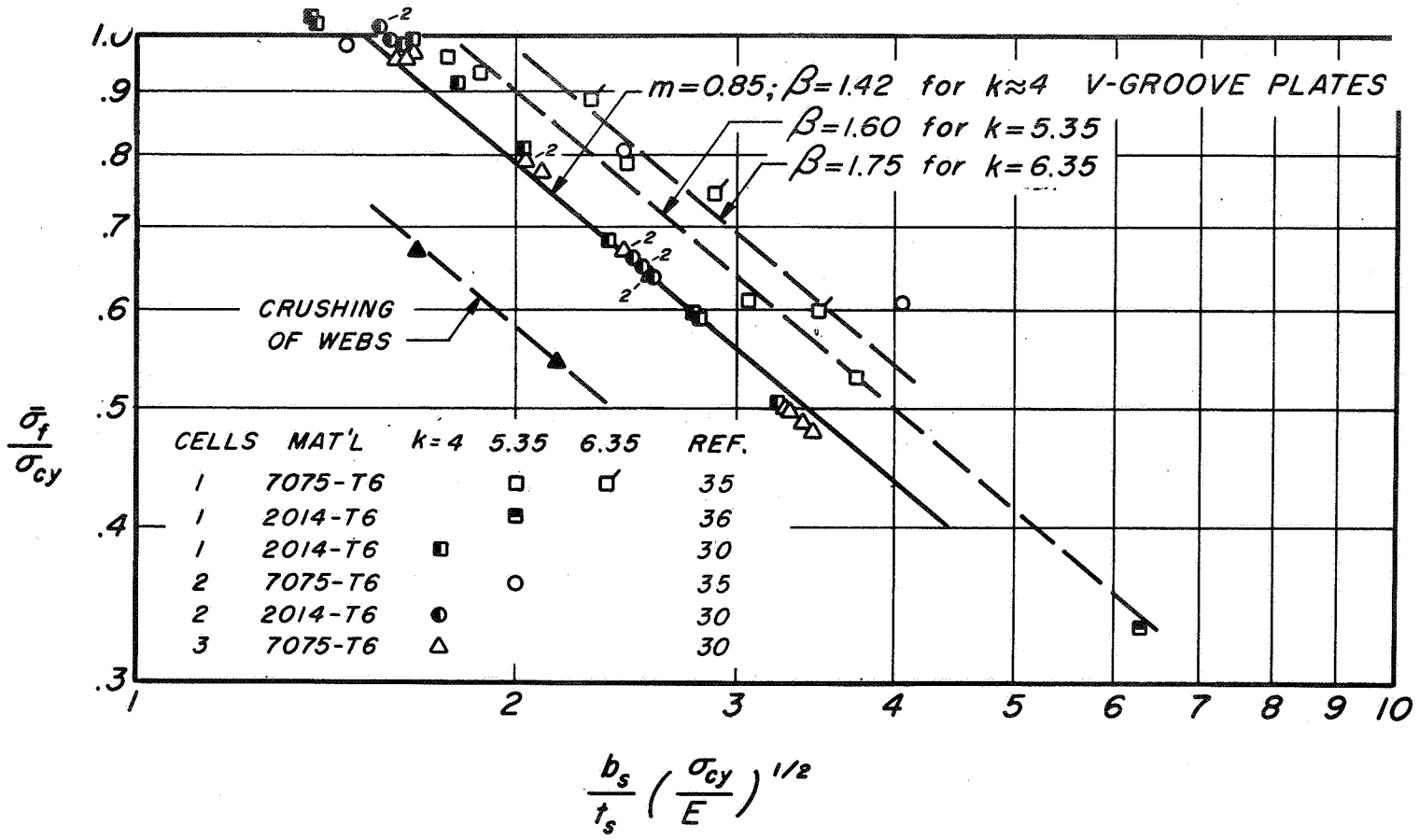

Figure 11.- Failing stresses of integral multiweb beams under bending.

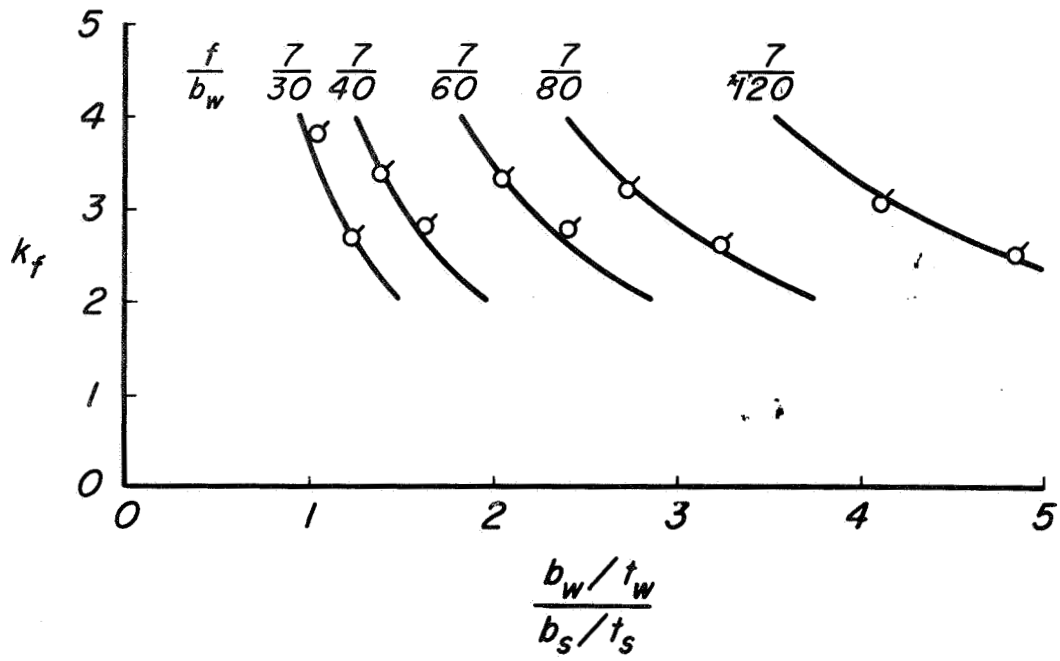

Figure 12.- Comparison of test data and theory for wrinkling failure of formed channel multiweb box beams under bending (ref. 33). $t_w/t_s = 0.41$ only.

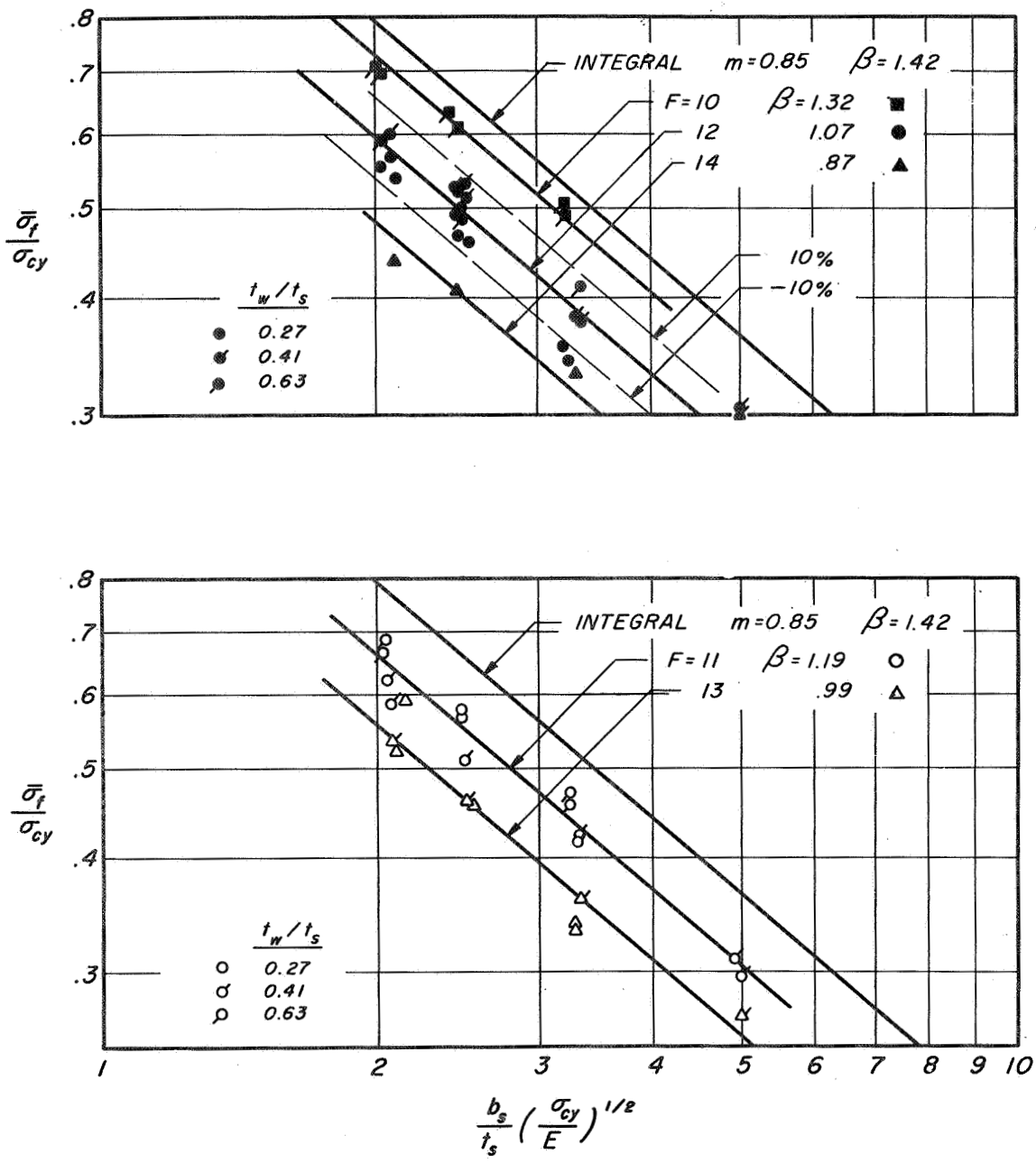

Figure 13.- Failing stresses of formed channel multiweb box beams under bending (ref. 34). $p/d = 3$; $r_w/t_w = 4$.

W-122

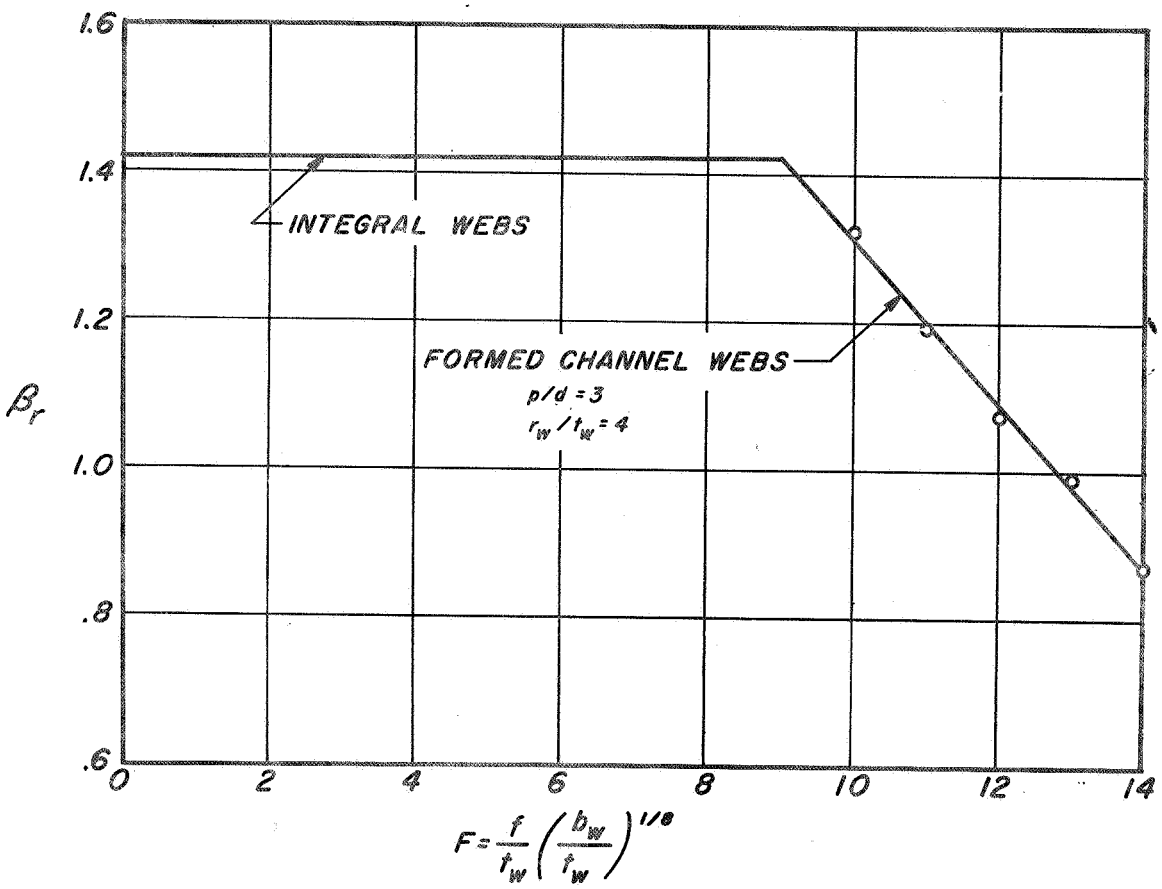

Figure 14.- Dependence of β_r upon F-parameter for formed channel multiweb beams.

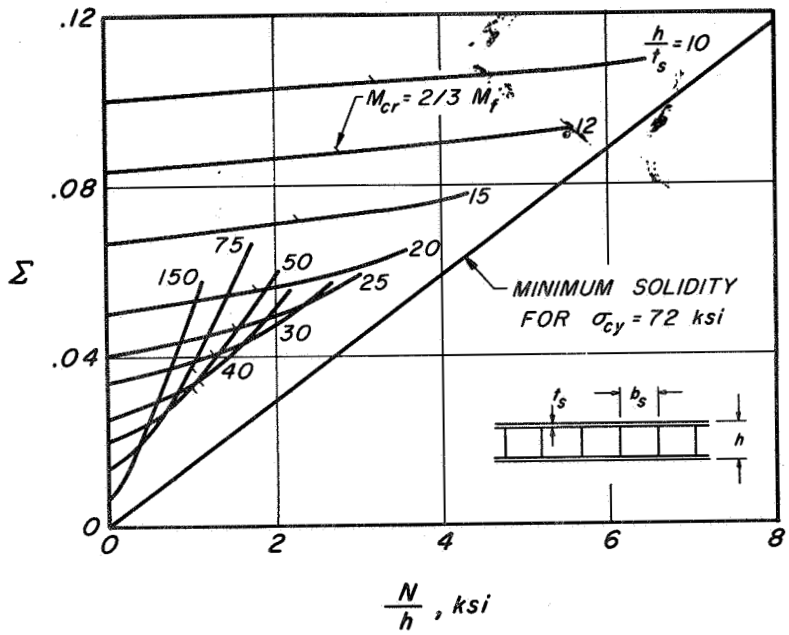

(a) Specified skin thickness.

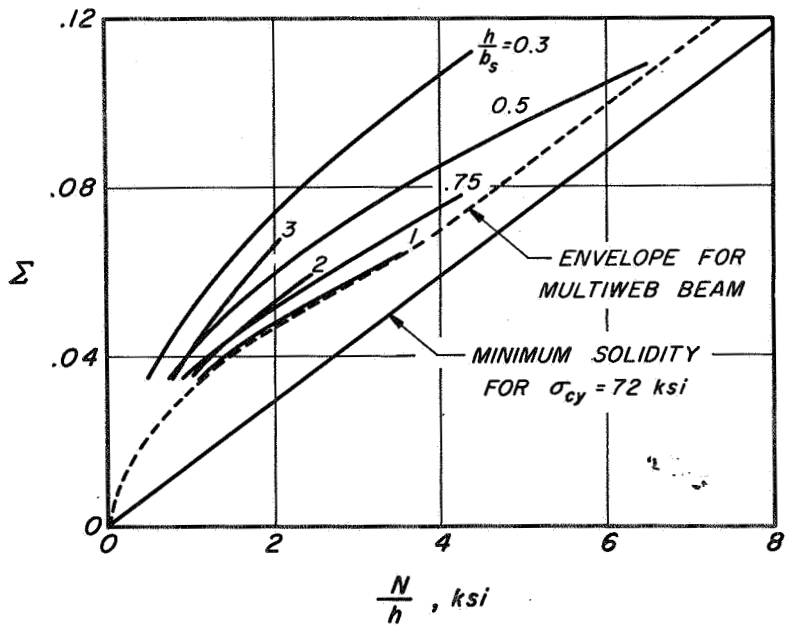

(b) Specified cell proportions.

Figure - Charts of integral-multiweb-beam efficiency for 7075-T6 aluminum alloy (ref. 30).

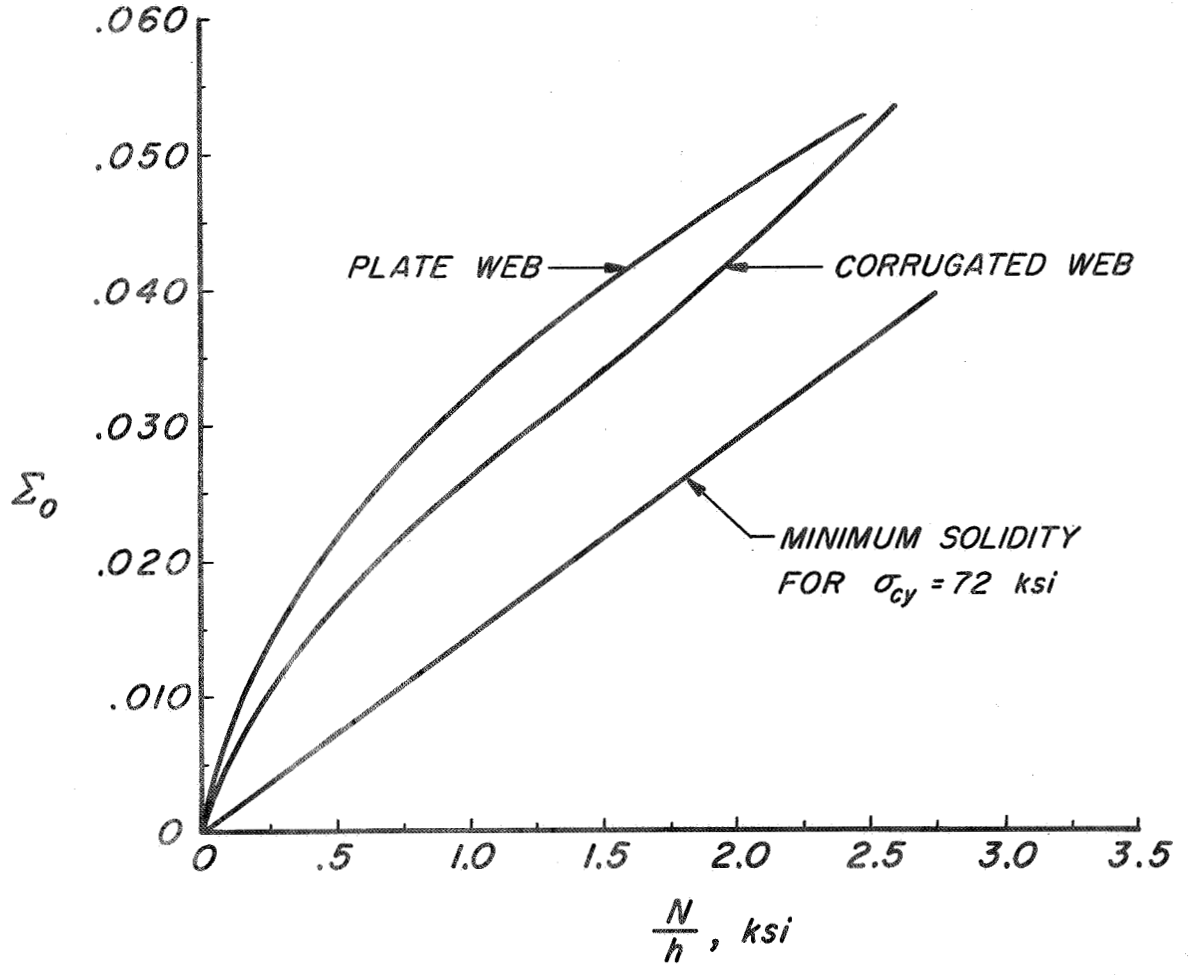

Figure 16.- Improvement in efficiency of multiweb beam in bending resulting from use of corrugated-web 7075-T6 aluminum alloy (ref. 40).

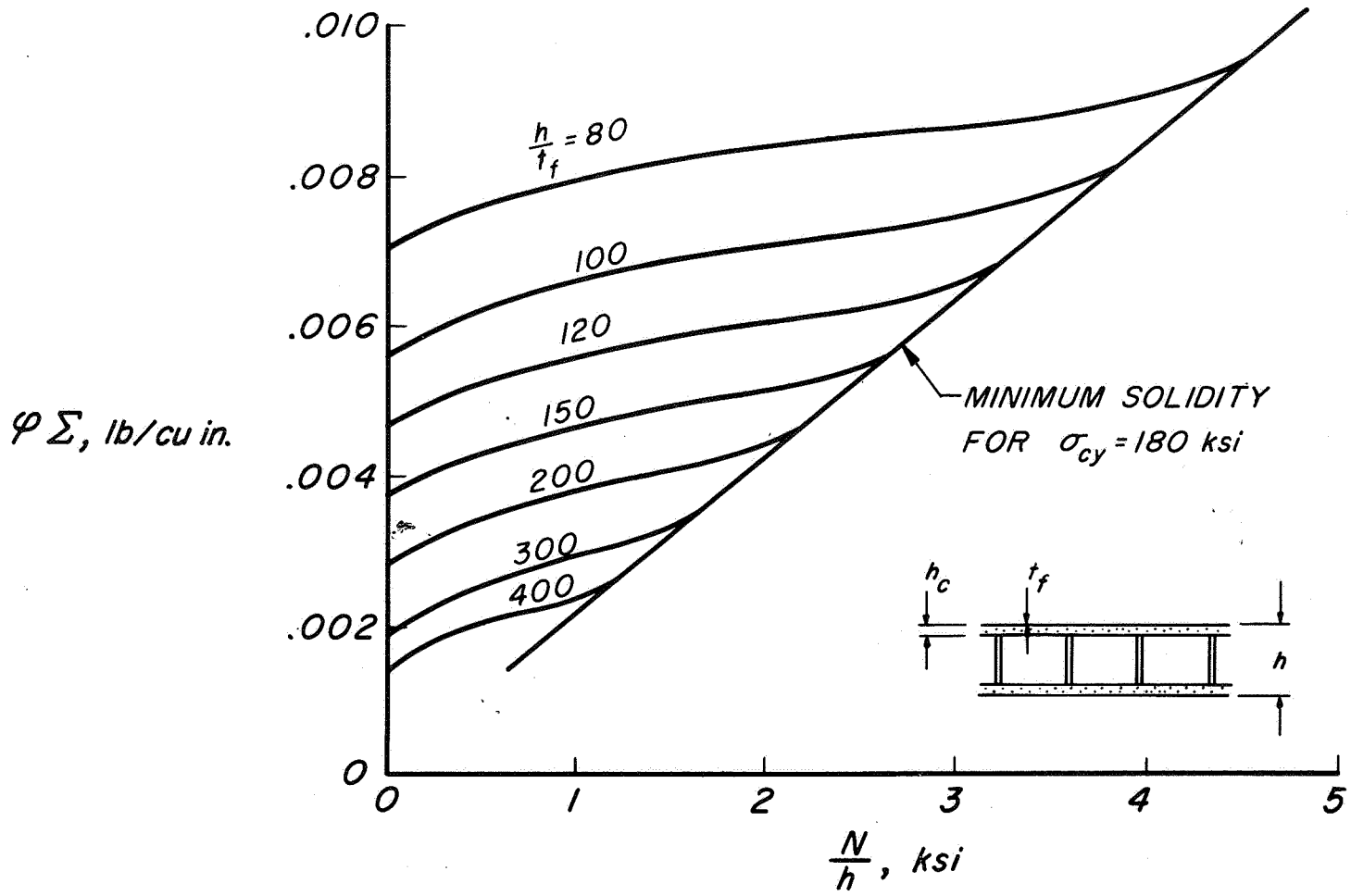

Figure 17.- Efficiency chart for stainless steel (17-7 PH TH 1050) sandwich cover with corrugated-web beam for specified skin thicknesses (ref. 41).

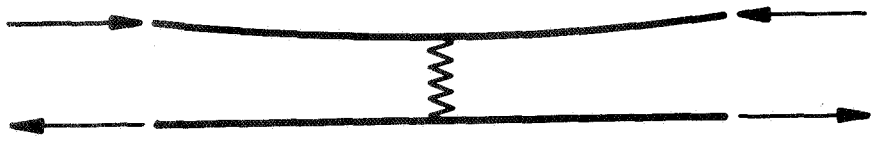

(a) Weak deflectional spring; strong flexural spring.

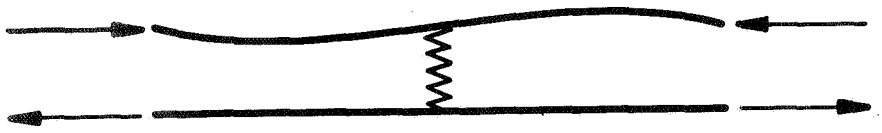

(b) Strong deflectional and flexural spring (effectively rigid).

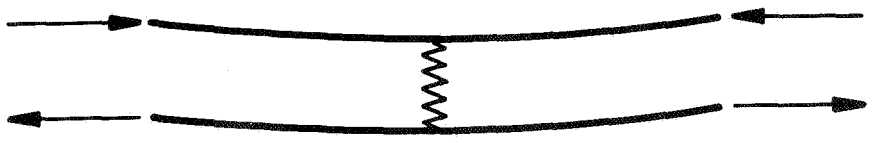

(c) Weak flexural spring.

Figure 18.- General buckling modes of a column supported by deflectional and flexural springs.

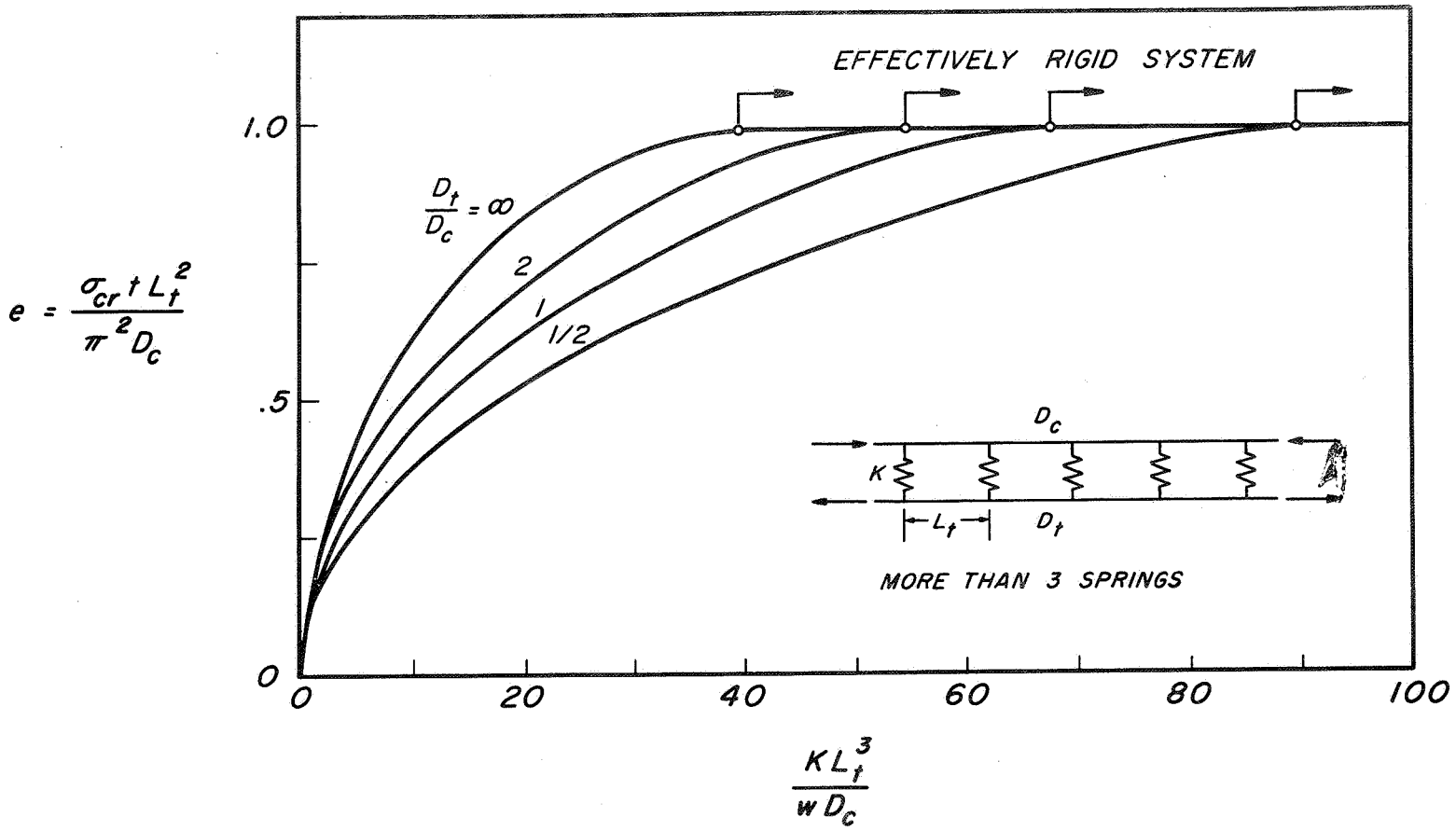

Figure 19.- End-fixity coefficient as a function of transverse stiffener parameter and relative flexural rigidity of wide columns (ref. 43).

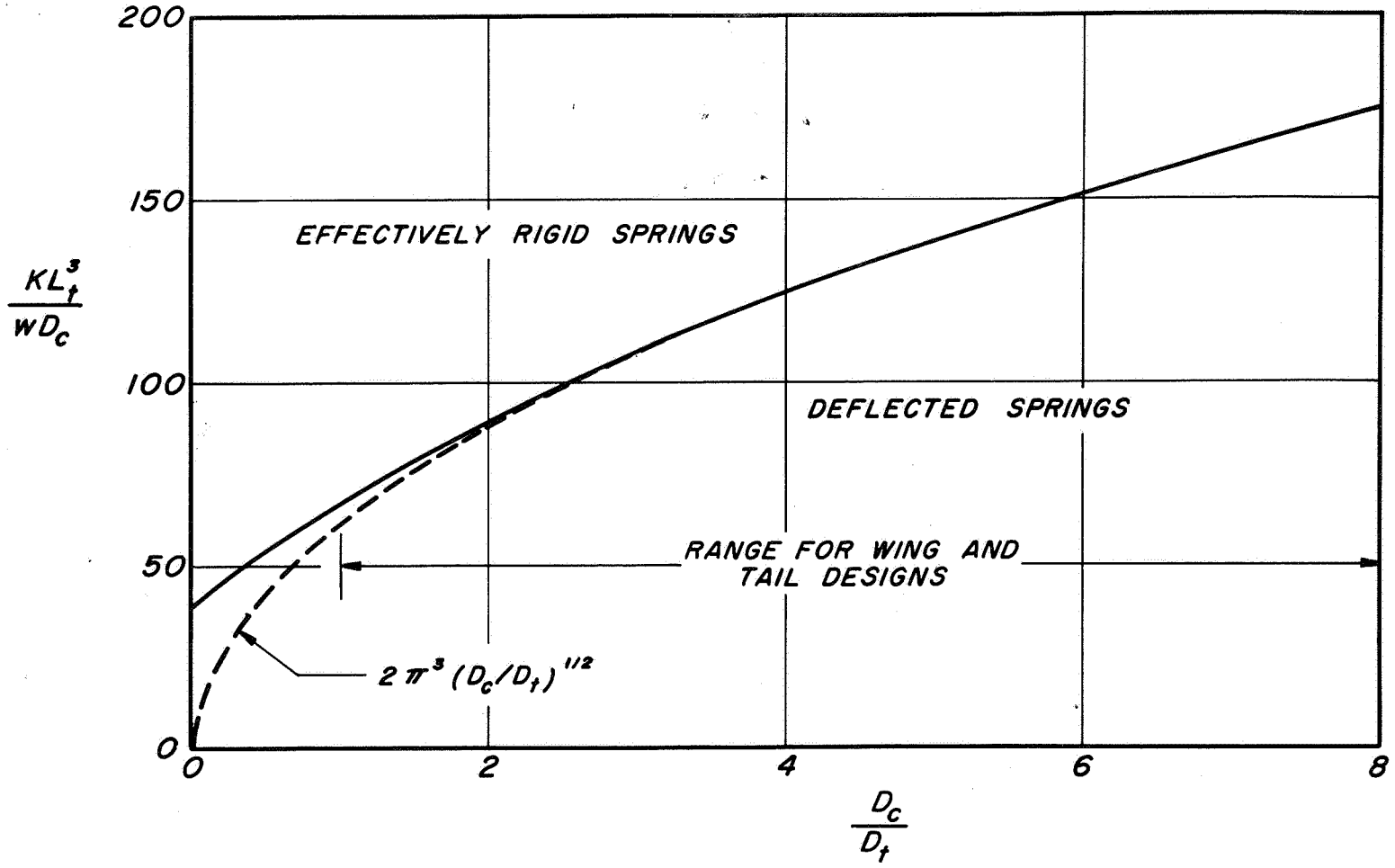

Figure 20.- Conditions for effectively rigid supporting system for wide columns (ref. 17).

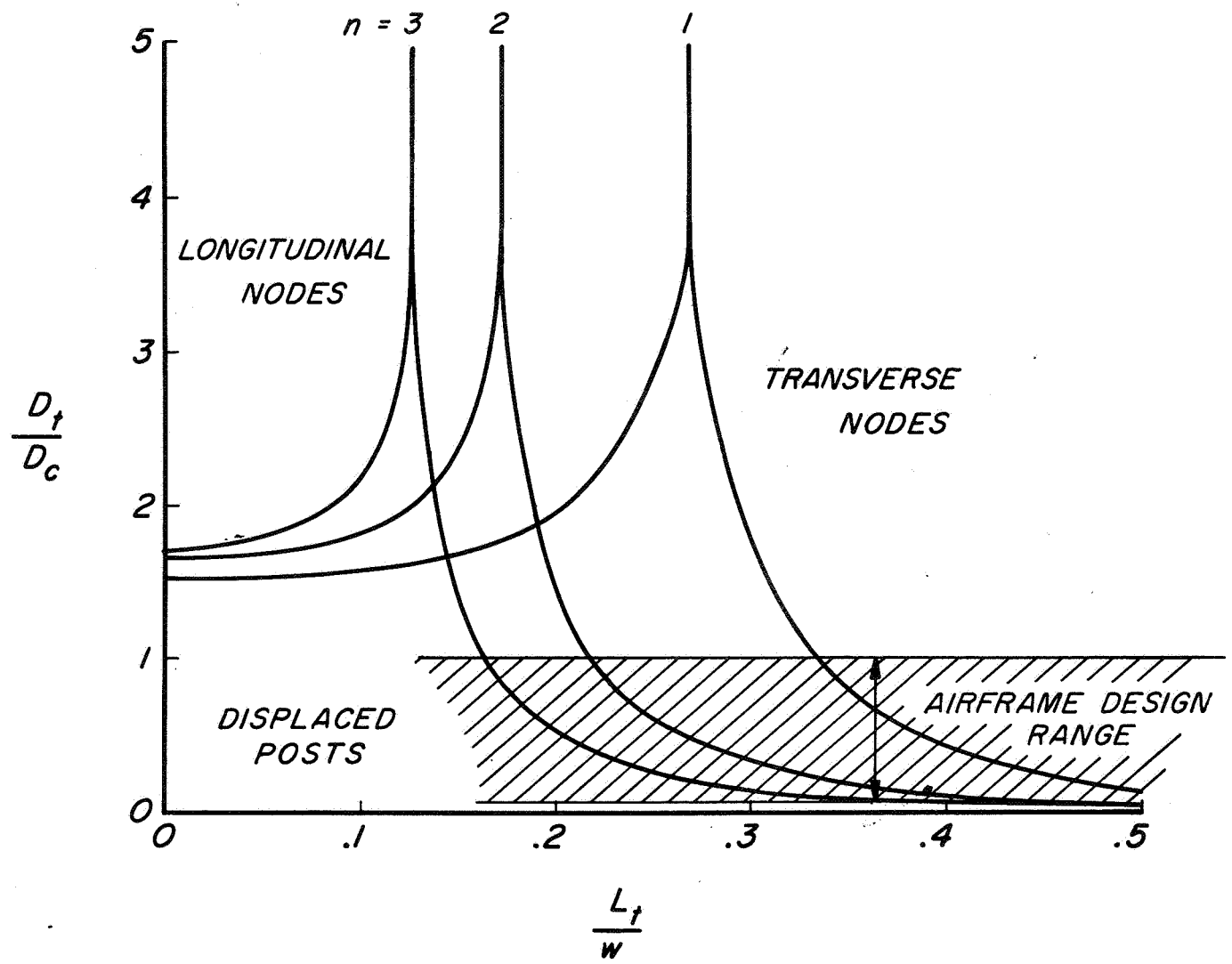

Figure 21.- Regions where post-construction buckling modes occur; effectively rigid posts (ref. 44).

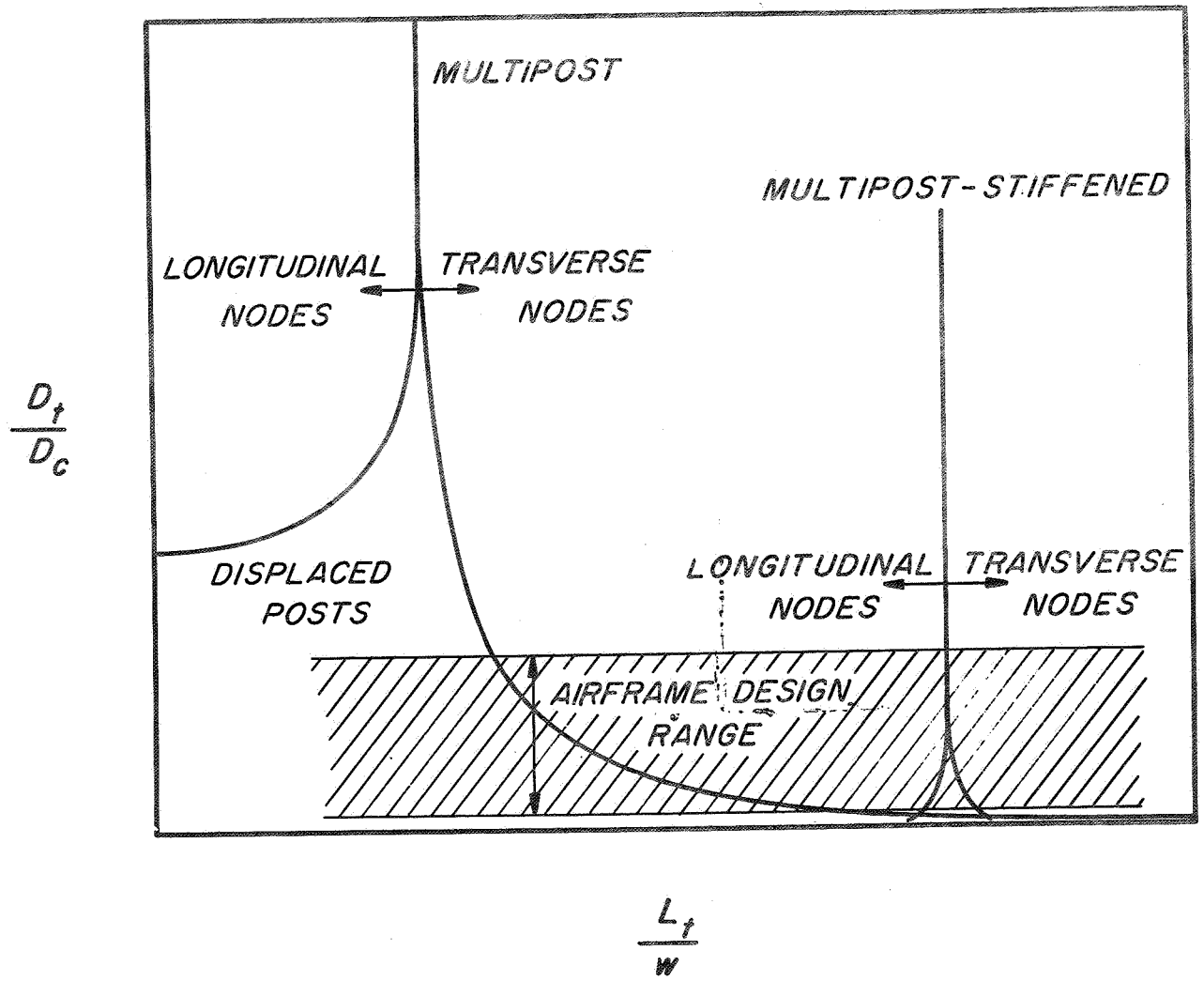

Figure 22.- Shift of buckling-mode boundaries for multipost-stiffened beams.

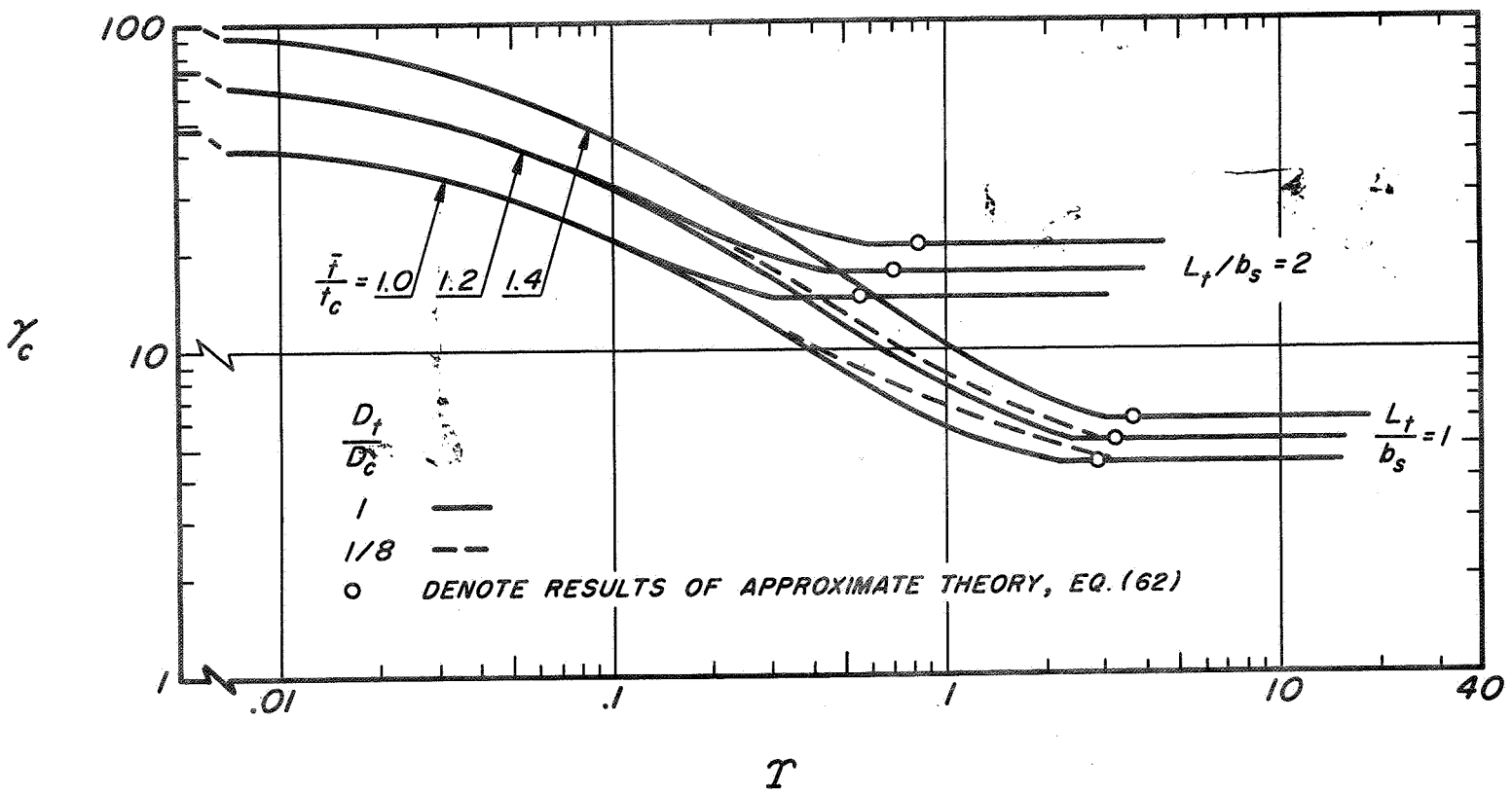

Figure 23.- Post and stiffener requirements to enforce longitudinal nodes for k = 4 (ref. 47).

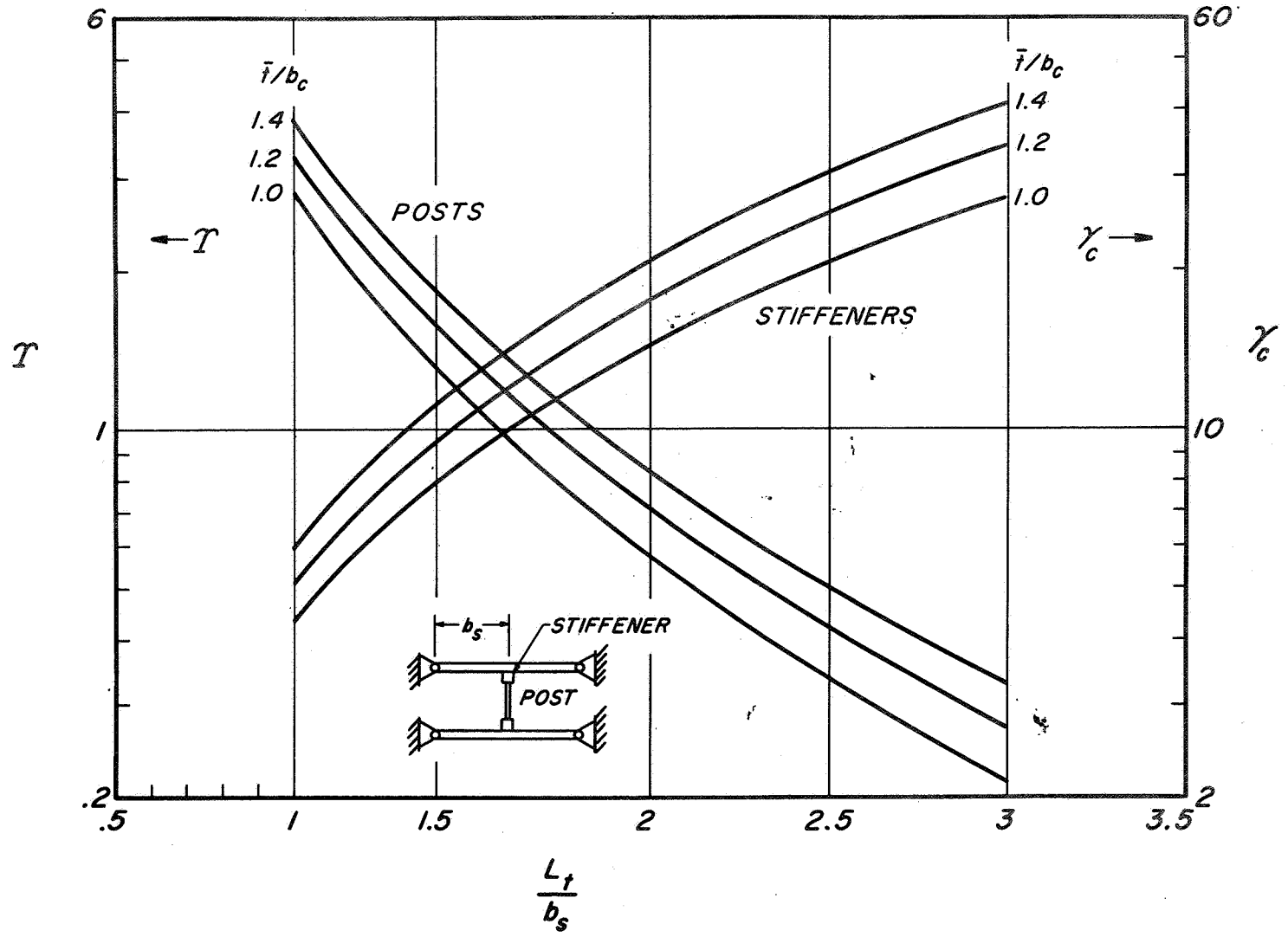

Figure 24.- Approximate minimum post stiffness corresponding to minimum stiffener rigidity to enforce longitudinal nodes.

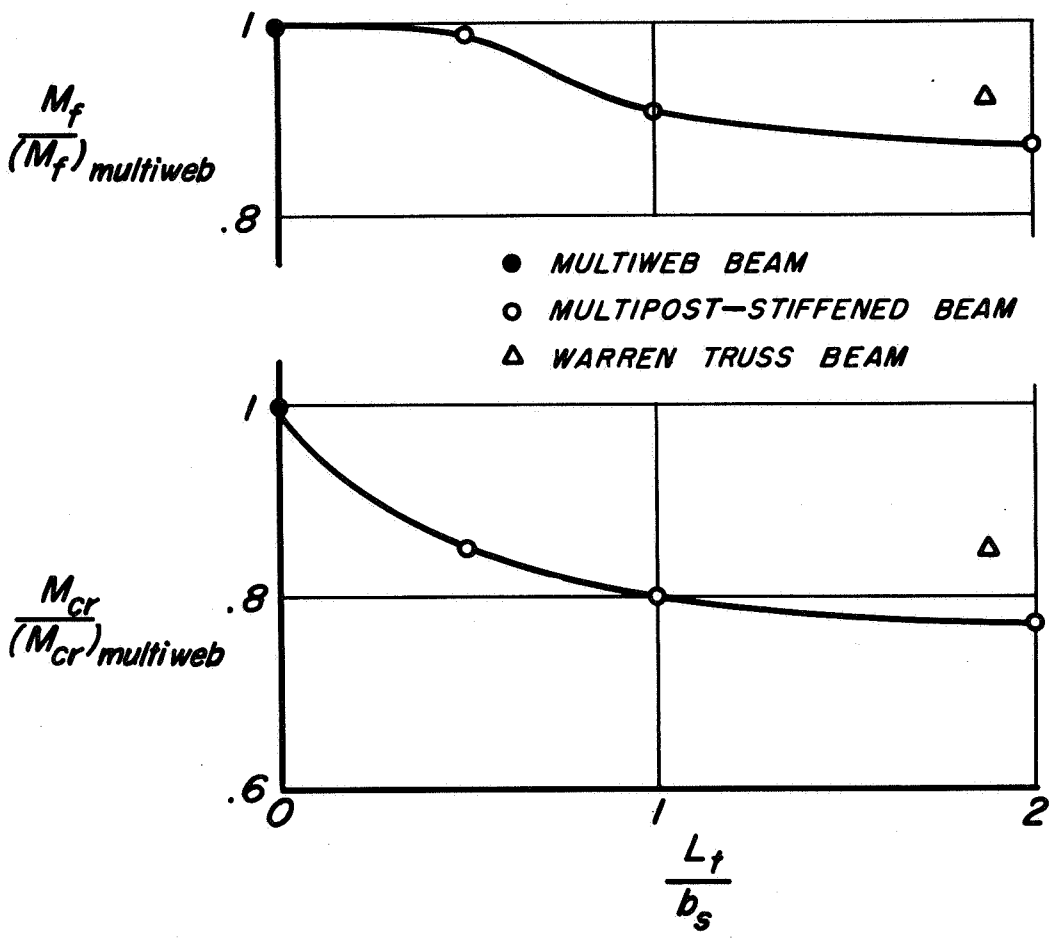

Figure 25.- Experimental data on buckling and failure of multipost-stiffened beams in bending compared with those of a multiweb beam (data of ref. 36).

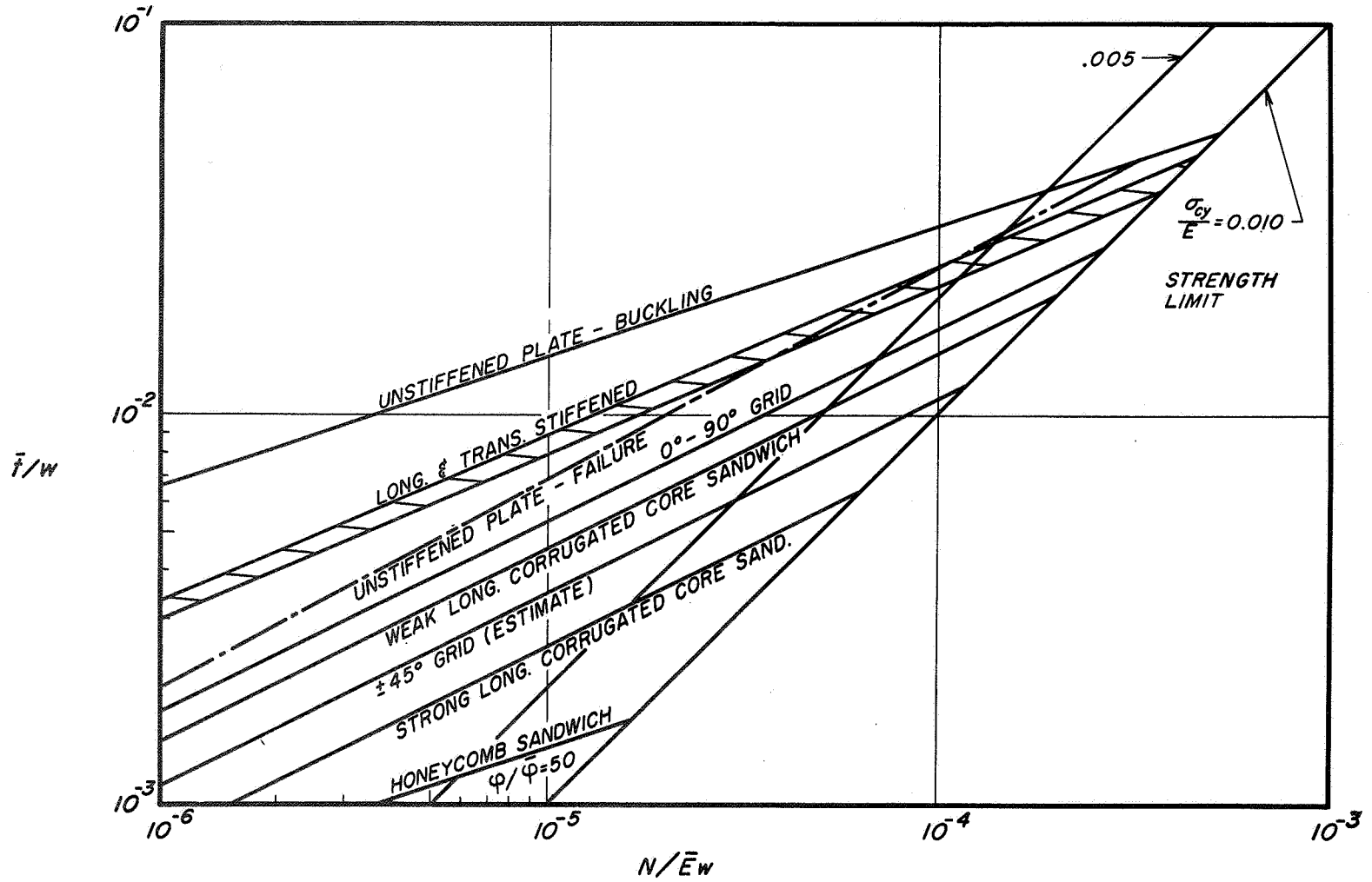

Figure 26.- Comparative structural efficiencies for compressive elastic buckling of long, simply supported plates (ref. 2). $\bar{E} = \bar{\eta}E/(1 - \nu_x\nu_y)$.

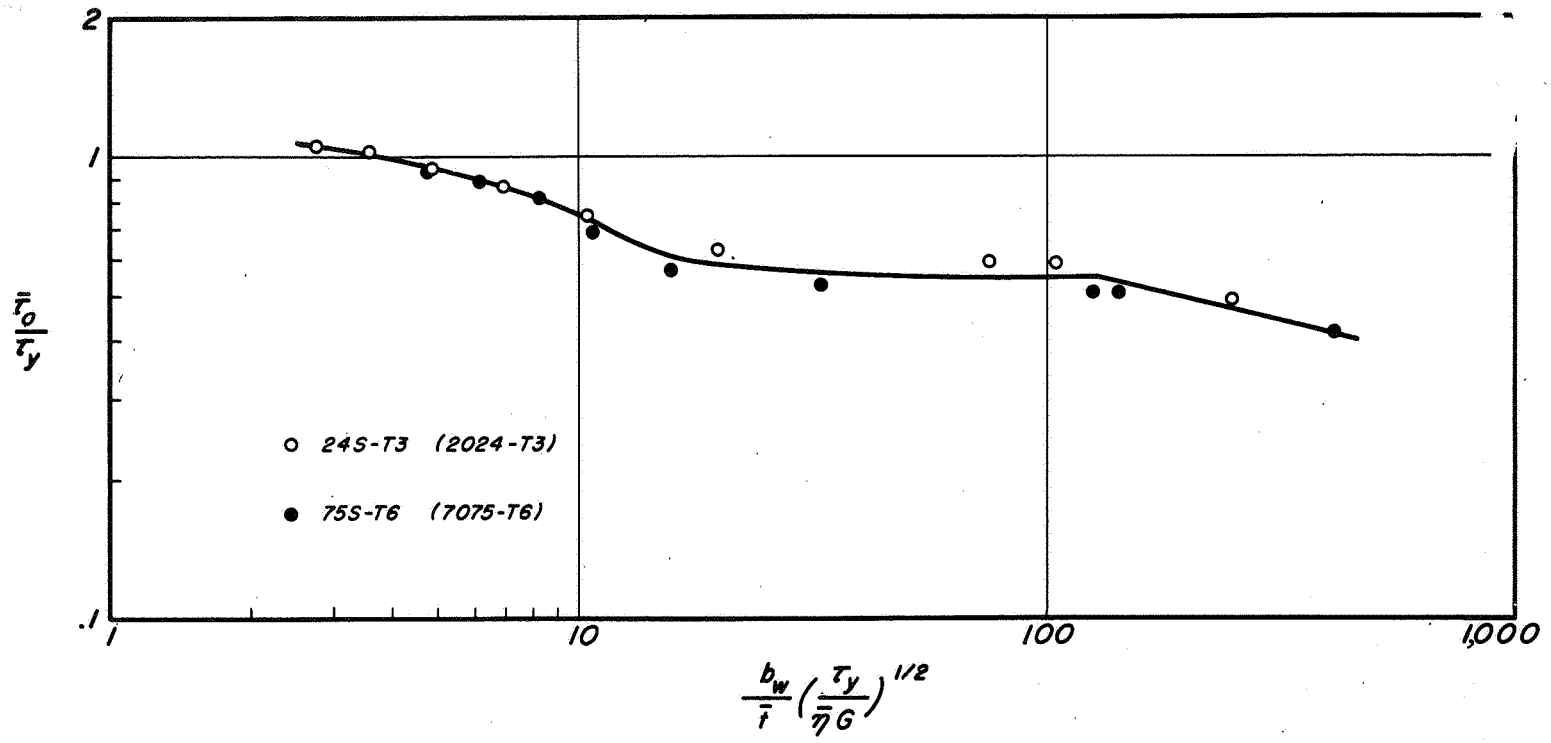

Figure 27.- Minimum-weight results for tension-field beams (data of ref. 49). $1/4 \leqq \frac{bs}{bw} \leqq 1$.

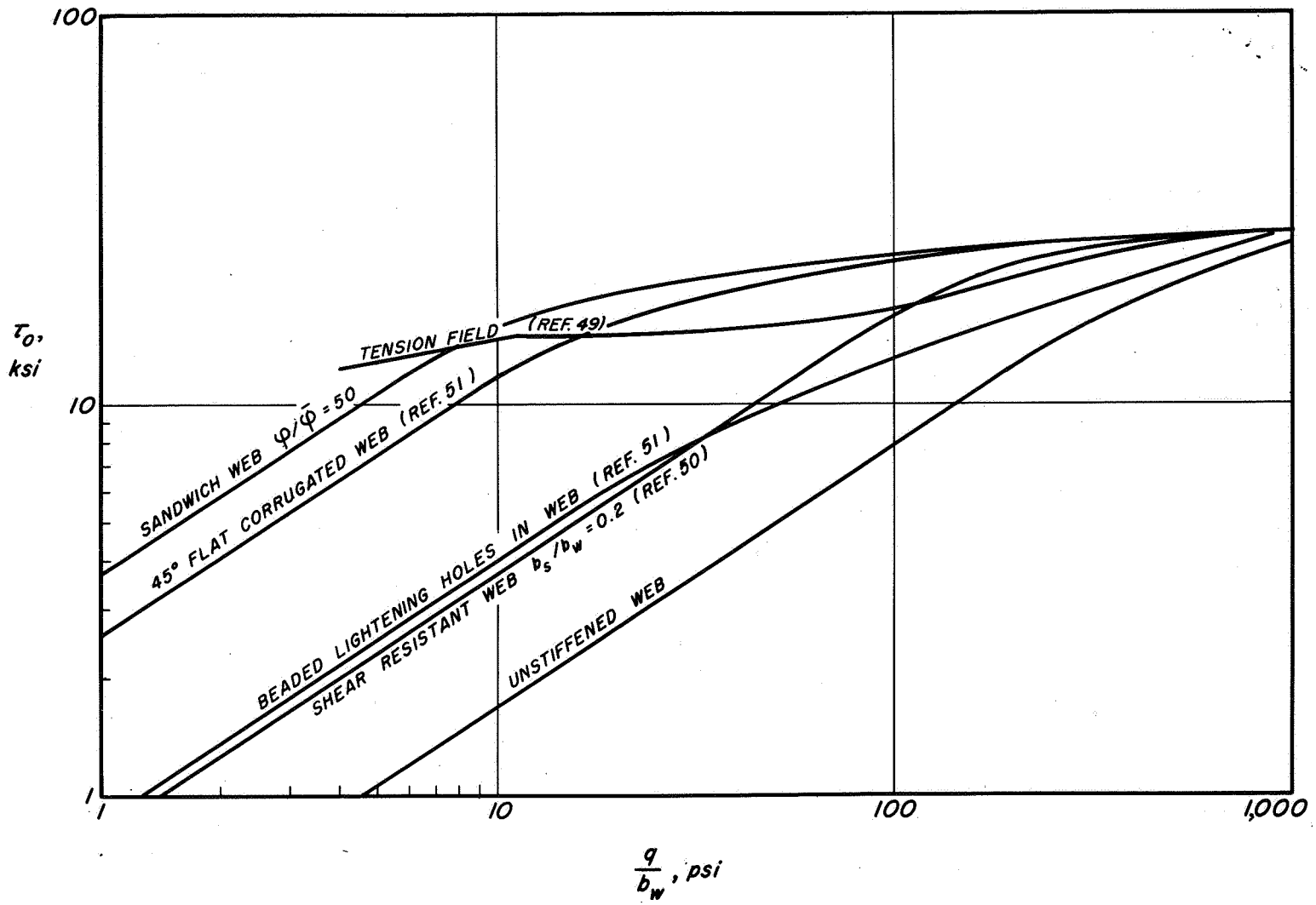

Figure 28.- Comparative structural efficiencies of shear-web systems of 2024-T3 aluminum alloy.

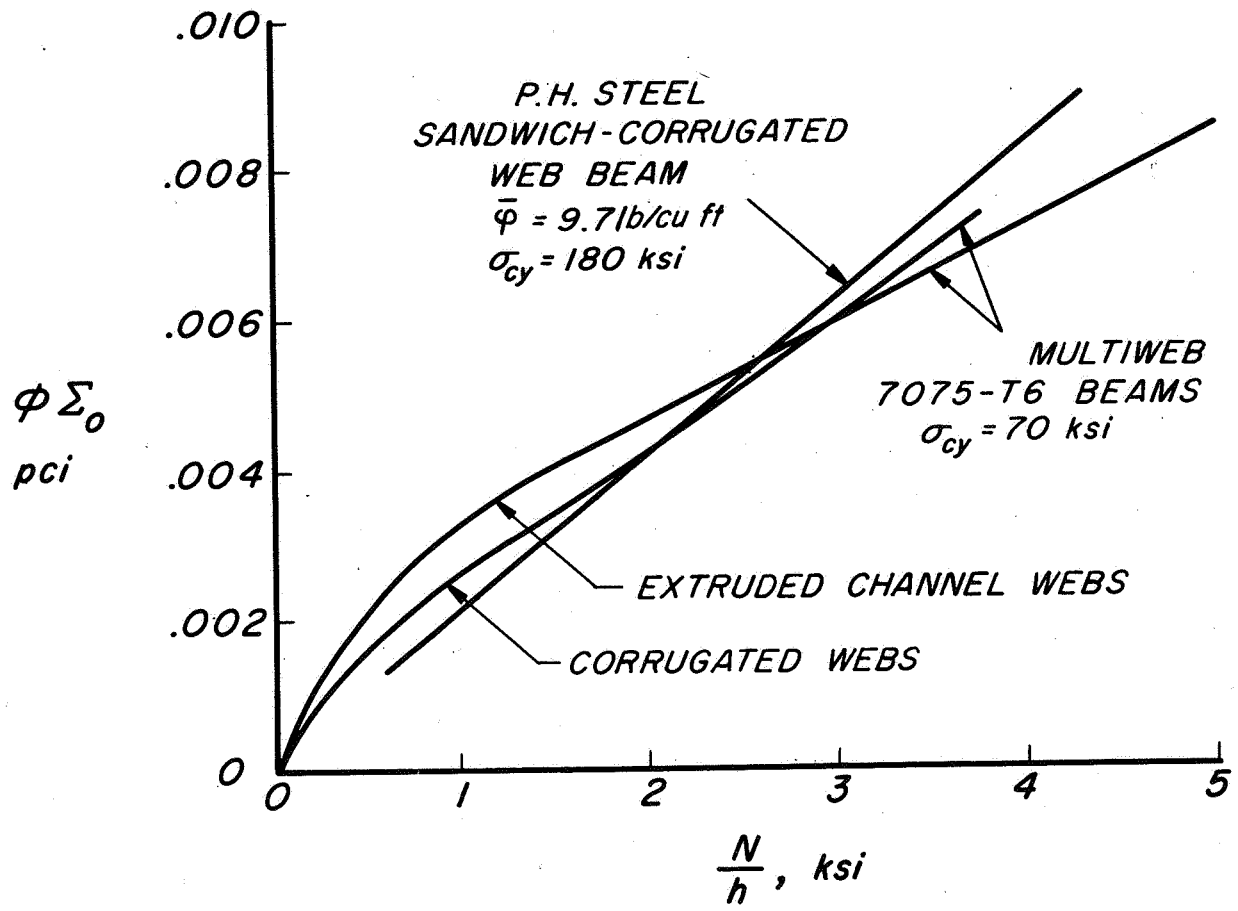

Figure 29.- Comparative efficiencies of several types of multiweb beams of minimum-weight design at room temperature (ref. 41).